Characteristics that matter in a climate façade: A sensitivity analysis with building energy simulation tools

Energy & Buildings 229 (2020) 110467

Contents lists available at ScienceDirect

Energy & Buildings

journal homepage: www.elsevier.com/locate/enb

Characteristics that matter in a climate façade: A sensitivity analysis with building energy simulation tools

Adrienn Gelesz [a,b], Elena Catto Lucchino [c], Francesco Goia [c,*], Valentina Serra [d], András Reith [a,e]

[a] Advanced Building and Urban Design Ltd, Budapest, Hungary
[b] Budapest University of Technology and Economics, Faculty of Architecture, Budapest, Hungary
[c] Department of Architecture and Technology, Norwegian University of Science and Technology, NTNU, Trondheim, Norway
[d] Department of Energy, Politecnico di Torino, Italy
[e] University of Pécs, Faculty of Engineering and Information Technology, Hungary

ARTICLE INFO

Article history:
Received 10 March 2020
Revised 2 September 2020
Accepted 6 September 2020
Available online 6 October 2020

Keywords:
Exhaust-air double skin façade (climate façade)
Sensitivity analysis
Different climates
Model validation
EnergyPlus
IDA ICE

ABSTRACT

Double skin façades (DSFs) are considered façade technologies that can reduce energy use and improve occupant comfort due to their advanced features. Their design requires reliable simulations due to their complex thermophysical behaviour, which are often carried out by practitioners using building energy software (BES) tools. Using an exhaust-air façade (also called climate façade) case study, the paper analyses the sensitivity of in-built DSF models in two popular BES tools (EnergyPlus and IDA ICE) for different orientations and climates. Small variations in input variables were considered to identify the parameters that the designer should pay most attention to during the design of the DSF according to different performance indicators. The results show that, regardless of the climate or orientation, the optical properties of the system (glazing and shading) were the most important in determining its performance, followed by the thermal properties of the glazing, while the geometrical, airflow and frame characteristics were less relevant. The model validation process also showed how differences in the in-built models (i.e. the use of a capacitance node for the glazed layers) lead to a difference in the reliability of the two BES tools.

1. Introduction

Double skin façades (DSFs) are building envelope systems that can reduce energy use and improve occupant comfort due to their advanced characteristics. A recent *meta*-analysis showed that the advantages given by these solutions can be up to 90% energy reduction potential, but when not properly designed or managed, an increase in energy use of up to more than 30% can be seen [1]. The large variation in performance is linked to the high complexity of these systems, which can often introduce non-optimal designs. This highlights the need to support the development, detailed design, and management of DSFs through advanced numerical tools.

Whole-Building Energy Software (BES) tools are meant for modelling and predicting the performance of an entire building including the interactions between its sub-systems. They are therefore particularly suitable to investigate how a DSF is integrated into the larger building energy concept, and how it can be dynamically controlled [2]. BES tools can be used at different stages of the design process to support the integrated performance design of both the building and single subcomponents and can provide informed support in detailing the characteristics of DSFs.

The research activity presented in this paper investigates the sensitivity of selected energy and comfort performance indicators to the DSF design parameters in two BES tools. The goal of the research is two-fold: i) to understand which are the most relevant construction parameters of this class of DSF that affect the energy and comfort performance of the façade using as case-study a climate façade; ii) to verify the extent to which the two selected BES tools produce coherent results concerning the importance of these parameters.

The target audience for the first part of this study is designers and researchers interested in the characteristics of climate façades and the factors that most affect their performance. This fills a current knowledge gap in the literature and can help practitioners to focus on the most relevant aspects of a DSF during the design phase when the exact design parameters of the system need to be set according to specific requirements like climate and orientation.

The second part of the study is aimed at helping consultants and developers working with BES tools to define reasonable expectations of the performance in two simulations tools, and assess the

* Corresponding author.
E-mail address: francesco.goia@ntnu.no (F. Goia).

https://doi.org/10.1016/j.enbuild.2020.110467
0378-7788/

Nomenclature

A_{inlet}	Area of the inlet [m^2]
α_{sh}	Solar absorptance of shading [–]
BES	Building Energy Simulation
DSF	Double Skin Facades
d_{cav}	Depth of the cavity [m]
d_{recess}	Recess depth of window (distance of interior window and building external plane) [m]
d_{sh}	Position of the shading measured from the external skin [m]
$d_{sh,gap}$	Ventilation gap around the shading [m]
e^{+}_{24h}	Area-specific daily heat gain [Wh/m^2]
e^{-}_{24h}	Area-specific daily heat loss [Wh/m^2]
f_{ext}	External frame fraction [%]
f_{int}	Internal frame fraction [%]
I_{tr}	Transmitted solar irradiance (on the vertical plan) [W/m^2]
h_{inlet}	Position of inlet measured from the floor level [m]
$\dot{q}_{LW,conv}$	Surface heat flux (includes long-wave radiative and convective heat flux) [W/m^2]
$\dot{q}^{+}_{tot}$	Total heat gain rate (includes short and long-wave radiative and convective heat flux) [W/m^2]
$\dot{q}^{-}_{tot}$	Total heat loss rate (includes short and long-wave radiative and convective heat flux) [W/m^2]
RMSE	Root Mean Squared Equivalent
ρ_{sh}	Solar reflectance of shading [–]
$S_i(t)$	Sensitivity index
$S_{i,d}$	Distance of sensitivity index
T_{glass}	Indoor surface temperature of the glass pane (inner skin, indoor-facing glass pane) [°C]
τ_{e,g_ext}	Solar transmittance of external glazing [–]
τ_{e,g_int}	Solar transmittance of interior glazing [–]
$\tau_{e,sh}$	Solar transmittance of shading [–]
U_{f_ext}	Heat transfer coefficient of the frame of the exterior skin including linear heat transfer coefficients of the glazing edge (Ψ_g) [W/(m^2K)]
U_{f_int}	Heat transfer coefficient of the frame of the interior skin including linear heat transfer coefficients of glazing edge (Ψ_g) [W/(m^2K)]
U_{g_int}	Center of glass heat transfer coefficient of interior glazing calculated at reference conditions (ISO 15099) [W/(m^2K)]
U_{g_ext}	Center of glass heat transfer coefficient of exterior glazing calculated at reference conditions (ISO 15099) [W/(m^2K)]
V_{cav}	Volumetric airflow rate in the cavity [L/s]

relevance of using these tools for the prediction of advanced façade systems. Readers interested in these aspects will find details about the validation work carried out through comparison with experimental data of two in-built modules for DSF simulations available in EnergyPlus and IDA ICE [3] in the Appendix. A critical analysis of the discrepancies between the results obtained in different tools is also provided, aiming to contribute to further developments of simulation models for advanced façade systems.

The paper is organised around four sections described hereafter.

In the Background section, we provide an overview of the current knowledge available in the literature, including previous activities where DSF systems have been modelled with BES tools and a sensitivity analysis to determine their key design parameters. We introduce the case study selected for the analysis, a so-called climate façade, with a description of its general features and its detailed characteristics (i.e. the actual façade chosen for the analysis). Finally, we provide the reader with a short introduction on the concept of sensitivity analysis and on the considerations used to select an appropriate method for this specific activity.

In the Materials and Methods section, we briefly report how the DSF has been modelled in two BES tools and the parameter settings necessary to run the simulations. We present the implementation of the local sensitivity analysis with details on the variables investigated and the three Performance Indicators (PIs) used in this phase namely the indoor surface glass temperature, the area-specific daily positive energy, and the area-specific daily negative energy crossing the façade.

In the Results and discussion section, we present the detailed outcomes of the sensitivity analysis in the BES tools. We reflect on how the resulting variability seen in the sensitivity analyses is linked to the differences in the two software tools.

The main findings of the study are summarised in the Conclusions section, which also highlights some limitations of the current study and the potential for future developments.

The paper also has two Appendix sections. In Appendix A, the main equations and explanation of the physico-mathematical models implemented in the two BES tools are described. In Appendix B, we present the validation of the modelling approaches and modules in the two software tools, including information on the experimental data collection and validation methodology. The reason for addressing these two topics in the Appendix is to keep the focus of the main body of the article on the key aspects of the study which are the role and the impact of the constructional and material properties of the climate façade on its performance.

2. Background

2.1. Simulations of DSF with BES tools

Many models exist for studying numerically the thermal performance of the DSF systems: analytical and lumped models, non-dimensional analysis, network models, control volume models, zonal approach, and computational fluid dynamics (CFD) [4]. DSF models in BES tools incorporate airflow network models integrated with a thermal network and a building energy model. These tools are particularly suitable as performance simulation tools to investigate the behaviour of DSFs in the framework of the overall building energy concept [2]. Different approaches can be adopted to study DSFs [5–7] and detailed analysis of the thermal and optical behaviour of DSFs can be carried out with more detailed simulation approaches (such as, for example, FEM and CFD [8–11]). BES tools have been widely used to simulate different types of DSFs primarily for the following two reasons: first to obtain a good balance between computational load associated with simulating a long period (usually one year) and the required accuracy to predict the overall performance of the façade; and second, the possibilities given by BES tools to test, in a quick way, different configurations and control possibilities for DSFs [12]. Examples of previous activities using BES tools to replicate the thermal behaviour of these façade systems includes simulations of almost the large spectrum of construction possibilities (e.g. [13,14]), as well as analysis of the advantages of DSF against single-skin façades [15,16]. In some cases [13,14,17,18], BES tools have been used to investigate the impact of the DSF's configuration on the thermal performance of the building. More parametric studies can be found in the litera-

ture if the search is not limited to simulations carried out with BES tools. In these studies, the parametric analysis is most typically focused on just one or a small number of parameters (e.g. cavity depth [13,19,20]; glazing U-values [13,20–24], glazing solar properties [13,21,23–26], the position of the shading [19,27] etc.), and in the majority of the cases, they only investigate a short period, e.g. single-day analysis with representative environmental conditions (either only winter or summer). The parametric analyses typically cover input parameters that illustrate different design choices and make also use of different methodologies (2D analysis [21,28], energy modelling [12,13,24,27,29], CFD [19,26], experiments [19], etc.) and boundary conditions. This variation of features, methods, and techniques makes it difficult to come to a general conclusion on the importance of one parameter over another. Some sensitivity analysis investigating the effect of small changes of a baseline [13,30] have also been performed but these studies are also characterised by a limited number of parameters. Studies that analyse different orientations are also rare, even though to reach a uniform architectural expression, fully glazed – especially high rise – buildings are in many cases constructed with the same type of façade on all orientations while allowing some flexibility in the actual specifications. While it is typical to limit the scope of the analyses to the South orientation, it has been seen previously that the summer overheating risk in the cavity is the highest on the West orientation [27].

The modelling of DSF systems in BES has some intrinsic limitations due to simplifications in the geometry and heat flow characteristics of components (inlet and outlet regions, enclosures around the cavity, shading) and the use of empirical correlations to solve some of the transport equations (especially the mass transport and convective heat transfer). This allows quickly obtaining useful information about bulk energy and mass flows without requiring high computational resources [2,7], although this might come at the cost of accuracy in prediction.

The reliability and precision of BES tools in replicating the thermal behaviour of DSFs have been addressed in a handful of previous activities, with sometimes contradictory results. EnergyPlus is among the most used BES tools for the simulation of DSFs, and consequently, it has been tested against experimental data in several studies. While some found a good agreement between the quantities calculated by the tool and the measured ones [31,32], for both single-storey and multiple-storey height DSFs, there are also studies showing a rather large discrepancy between simulations and experiments [17,33]. Such differences might be linked to the use of a calibration procedure. The adoption of this procedure, which can be legitimately used to reduce the uncertainty in the inputs of the models, may, however, lead to an overestimation of the performance of the BES tool in terms of validation. In most cases, the validation with experimental data only concerned the comparison of the simulated indoor glazing surface temperature and/or the temperature of the air gap and left out the tool's capability to replicate other relevant quantities that affect the total performance of the system. The literature available on the modelling possibilities given by EnergyPlus also reflects the two possible approaches of modelling a DSF, i.e. as a series of stacked thermal zones [17,31,32] or a dedicated "airflow-window" module embedded in the tool [33].

Both possibilities of modelling DSFs are also given in IDA ICE [34]. Examples for the use of the in-built module can be found in the literature [12,35], but only a couple of experimental validations are available. This software tool has been assessed approximately ten years ago, in an extensive inter-software comparison [36], and more recently by the same author of this paper [3]. The latter validation activity forms the basis of the extended validation presented in this paper, where the reliability of the software tools has been assessed not on the single thermo-physical quantities (temperature, heat fluxes, solar irradiance values), but on the aggregated, daily values of total transmitted energy through the façade, as more comprehensively described in Appendix B.

2.2. Climate façade (mechanically ventilated exhaust-air façade)

Several types of DSFs [29] present different characteristics in geometry, materials, ventilation mode, and air-flow modes. The case study façade selected for this investigation is an exhaust-air façade, which consists of one storey-high, mechanically ventilated elements that are juxtaposed on the façade. In these façades, the air typically enters from the indoor environment in the lower region of the façade through an opening in the frame and leaves the cavity at the upper part of the façade, either expelled to the outdoor environment (Fig. 1 a) or extracted through a duct as part of the HVAC system (Fig. 1 b) – and in the latter case, it takes the name of "climate façade".

Because the façade can be considered a part of the ventilation plant of the building, the operation in terms of airflow rate is rather constant, both in winter and summer conditions. This means that the possibilities to play with the airflow rate to remove a greater or smaller amount of heat from the cavity is usually not adopted as the airflow rate is linked to the volume of air supplied to the room for ventilation purpose.

A screen or venetian blinds in the climate façade is an important element to promote the exploitation of the solar heat gain through the ventilation airflow, to prevent indoor discomfort due to the excess of luminous gain, and to avoid excessive cooling loads due to direct solar gains to the room. In practice, the use of the shading element is necessary most of the time to ensure that the direct solar gain and the luminous flux on the user is not creating uncomfortable conditions.

2.3. Local sensitivity analysis

Sensitivity analysis is the study of how uncertainty in the model outputs can be allocated to the uncertainty in the model inputs [37]. It is a technique widely used across different fields such as ecology, chemistry, material science, economics, and energy modelling [38–41].

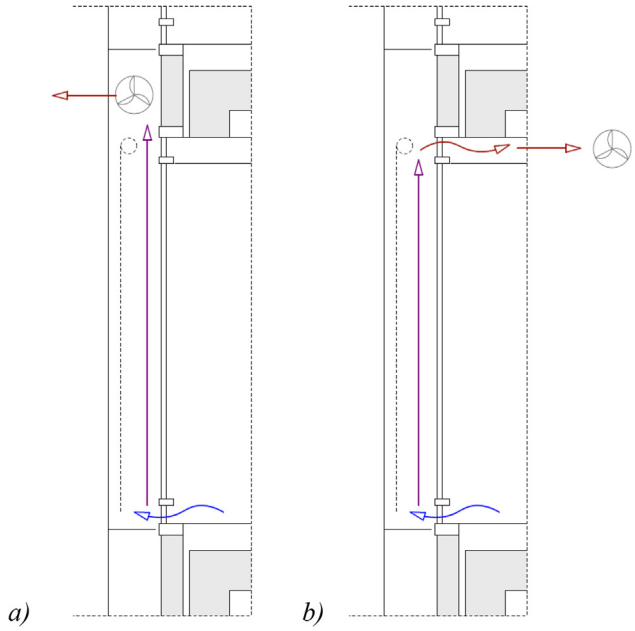

Fig. 1. Sections of exhaust-air façades a) air exhaust façade b) climate facade.

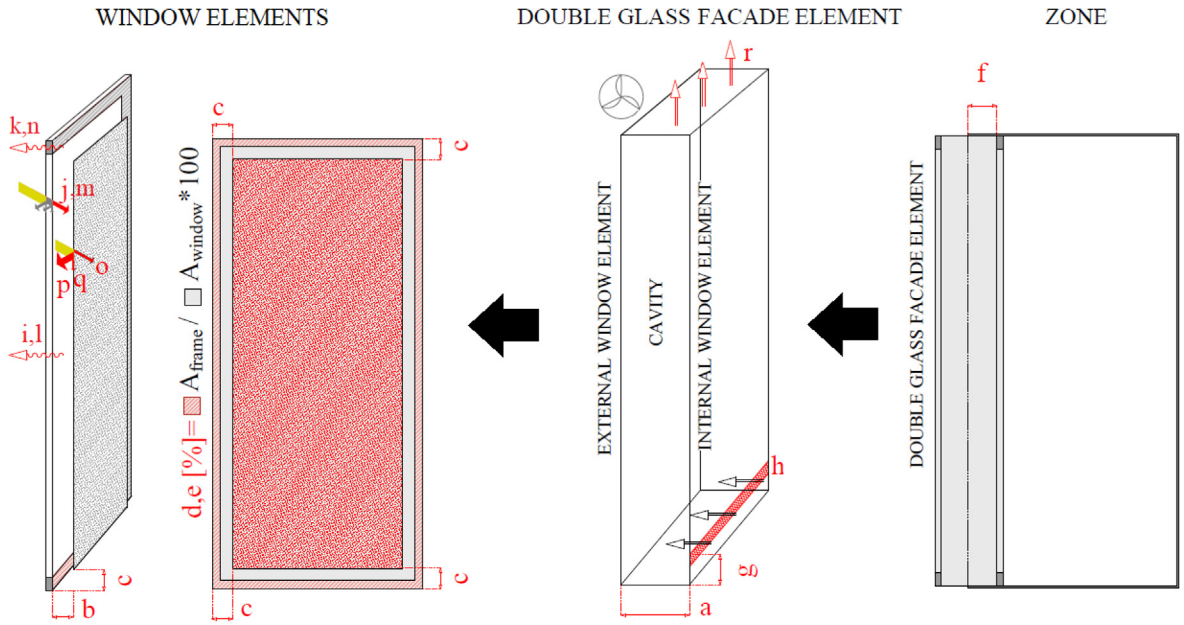

Fig. 2. Schematic of parameters defined in Table 2, view, axonometric view and section: a) IDA ICE b) EnergyPlus.

Many types of sensitivity analysis techniques exist but all return a list or a "sensitivity ranking" of the input parameters according to their influence on the outputs of the model. As each sensitivity analysis technique results in a slightly different sensitivity ranking, the actual ranking is not as important as much as is the determination of the key parameters to which the model is most sensitive [42]. From a practical point of view, the parameters consistently appearing near the top of the list will be the ones which are the most sensitive and require the most attention.

In this paper, a local sensitivity analysis is implemented using the so-called "One-At-A-Time" (OAT) technique, which consists in changing each parameter individually. This approach is useful to assess the impact of parameters in a model that contains *n* factors with a relatively small number of simulations, equal to *n + 1*. However, the non-linear effect in the output variation due to a combination of two or more variations in the inputs, cannot be studied with this method. One must then use a global sensitivity analysis that can assess the effect of multiple combinations of input variations [43].

Global sensitivity analysis techniques return a more comprehensive understanding of the general picture compared to local sensitivity analyses but require a much higher computational cost. The choice of the method to be adopted in a sensitivity analysis study heavily relies on considerations of computational time versus aims [44]. Local sensitivity analysis is a computationally efficient screening method proven to be a reliable strategy if the purpose of the analysis is to identify a cluster of input parameters most sensitive to the model output variability [43]. Because part of the scope of the research presented in this paper is to adopt a method that can be replicated by practitioners during the design phase when computational cost must be minimal, a method based on local sensitivity analysis was deemed more appropriate and selected for the analysis. This choice is also supported by indications in the literature showing that different sensitivity analysis methods can, to a large extent, identify the same cluster of most sensitive input parameters [37] as a global sensitivity analysis, and is still a very useful technique because of its simple implementation, low computational costs, and easy interpretation [40].

While, technically, the local sensitivity analysis must satisfy the condition of linearity to be applicable, the relationship between the outputs and the inputs in the case of the thermal simulation of DSF may be strongly non-linear. However, by making use of relatively small variations around the baseline input values, the linearity requirement around the point of investigation is, based on our experience on modelling approaches implemented in BPS tools, satisfied and the technique can be used with a high degree of confidence. The correctness of the approach is also justified by its popularity in the scientific literature and wide adoption for local sensitivity analysis using BES tools [37,44]. The remaining challenge associated with adopting this technique is the identification of the largest magnitude of the perturbation that can be used and satisfies the condition of linearity. This topic alone would require a comprehensive discussion that goes beyond the scope of this paper. However, as explained more in the following section, different perturbations have been tested in this analysis to ensure the robustness of the outcome of the analysis.

A final remark concerns the conceptual comparison between a parametric analysis and a sensitivity analysis. While a local sensitivity analysis is suitable to give information on the relative order of importance of different parameters, a parametric analysis, e.g. [14,18], is more suitable to investigate the optimal design choices within a given domain of possibilities. In an ideal design or research process, the sensitivity analysis is developed prior to the parametric analysis to initially reduce the numbers of parameters that later need to be investigated by identifying those that have a larger impact on the selected simulation output.

3. Materials and methods

3.1. Building energy simulation tools

BES tools either include dedicated models for DSF elements or allow the modeller to define DSFs as thermal-airflow networks. Two widely popular BES tools, EnergyPlus (version 9.1) and IDA Indoor Climate and Energy (IDA ICE) (version 4.8) incorporate in-built models for DSFs and have been selected for this investigation as the models most likely to be selected by practitioners during the design phase. In-built models are specific models that allow the user to directly enter specific input information that is then used to modify the heat balance of the window following the consideration that a ventilation flow is provided between the glass panes without requiring any additional modelling effort from the user.

The in-built models also allow sometimes users to pick between different levels of complexity for the description of the thermal and optical properties of the glass panes and frame constructions, and in this study, the more complex approach was selected as far as allowed by the BES tool.

A more detailed description of the dedicated sub-routines and the physical–mathematical models implemented in the two BPS tools is reported in Appendix A.

3.2. Experimental validation of the modelling approach in the two software tools

Experimental data collected during a long-term measurement campaign on a test cell facility was used to validate the two in-built models of DSFs available in the two BES tools considered for this study. More information about this procedure is given in Appendix B. The results shown in this paper are an extension of the ones previously reported in [3] and aggregate simple measured physical quantities into Performance Indicators (PIs). The measured values of solar radiation, indoor and ambient temperatures and indoor surface temperatures were used to recreate the real boundary conditions in the simulations by modifying the weather data file used by the simulation tools. The solar radiation was calculated from the values of outdoor solar irradiance measured on the horizontal and vertical plane. The outdoor air temperature was used in the custom weather files, while indoor temperatures were given as setpoints within the models. Indoor surface temperature measurements were also imposed in the models using schedules and applied to the corresponding surfaces within the models. In EnergyPlus, this was given directly as a set value for the surface temperature node. This approach was not possible in IDA ICE and instead, the same result was achieved by creating an additional conditioned zone around the volume of the cell delimited by fictitious surfaces. The air temperature inside this new zone surrounding zone was controlled using setpoints that matched the measured temperatures and recreated the experimental boundary conditions, as described in [3].

Summarising the results presented in Appendix B, the validation of the modules in IDA ICE and EnergyPlus revealed a series of mismatches in the prediction of internal glass surface temperatures and daily heat gains and losses. Despite these disparities, the tools could predict the main features of the time profiles in terms of peaks, valleys, and intensities, as well as the trends in surface temperatures, and energy loss and gain for double skin façades. The software tools also provided a more convincing performance in terms of matching the experimental data when the shading device in the DSF was lowered compared to when the DSF was simulated without the shading device, where much greater deviations between simulation and experiments can be seen. This suggests that the results of the sensitivity analysis were robust for configurations with the shading devices activated; but for configurations without the shading device, the reliability of the analysis cannot be fully ensured because of the discrepancies seen between simulations and experimental data. The validity of the analysis is, however, maintained by the fact that for optimal DSF operation, the shading device should be activated frequently both to ensure thermal comfort and to ensure a suitable visual performance for the

highly glazed façade which is subject to a risk of glare in most orientations.

Finally, the model in IDA ICE generally captured the time profiles more accurately, while EnergyPlus showed a shift in the profiles due to the lack of a heat capacity node for the glazing. This difference in the features of the two in-built models also has implications for the general reliability of EnergyPlus versus IDA ICE.

3.3. Settings of the sensitivity analysis

After checking the reliability of the simulation tools with the experimental data, a general model for the room and the façade was defined for the sensitivity analysis. Except for the walls incorporating the DSFs, all other surfaces were modelled as adiabatic and not interacting with the surroundings. The indoor air temperature setpoint value was changed for the different seasons and equal to 20 °C in Winter (January-February; November-December), 23 °C in Spring and Autumn (March-April; September-October), and 26 °C in Summer (May-August). This choice was done to minimise the impact of the differences that can occur within the two simulations at the whole building/room level on the sensitivity analysis at façade scale. By keeping constant the indoor air temperature, the discrepancies seen in the sensitivity analysis between the two software tools were then only due to the differences in the modelling of the façade.

The orientation of the office room was set so that the DSFs were exactly aligned with one of the four cardinal directions each time. The simulations were run in three different climates to assess whether the different outdoor boundary condition influenced the results of the analysis. The three climates were selected to be representative of different boundary conditions: Torino, located in a humid subtropical climate (Cfa according to the Köppen-Geiger climate classification), which is where the validation case study was located; Oslo located in the warm summer continental climate typical of Northern Europe (Dfb); and Hong Kong, located in a dry-winter humid subtropical climate (Cwa).

In total, 18 parameters likely to be considered by the designers or consultants planning the DSF's configuration during the design phase were selected for the sensitivity analysis (Table 1). Although the cavity height is considered to affect the results, this was not assessed, as this parameter is dependent on the floor height, which is usually a basic input given to the façade consultant by the design team.

The perturbation (variation) was set to ±10% for each parameter around the baseline case (Table 2) after testing different perturbation intervals (±5% and ±25%) on a few selected orientations and one climate to verify the robustness of the selected approach. This analysis yielded similar values to those obtained with the selected ±10% variation, thus confirming the relevance of the selected approach.

The effect of the perturbation was assessed using three PIs:

- the indoor surface glass temperature (T_{glass} [°C]);
- the area-specific daily positive energy (e^{+}_{24h} [Wh/m^2], daily heat gain) crossing the façade;
- the area-specific daily negative energy (e^{-}_{24h} [Wh/m^2], daily heat loss) crossing the façade.

These PIs aim at understanding the impact of the design choice on the thermal domain. The equations for calculation of e^{+}_{24h} [Wh/m^2] and e^{-}_{24h} [Wh/m^2] can be found in Appendix B of the paper.

The choice to focus the sensitivity analysis on PIs that address the thermal and comfort performance of the façade was done to limit the scope of the research, and to ensure that the results obtained could be as general and as interesting as possible. A sensitivity analysis focused on the impact on the visual environment of the different DSF's configuration would have lacked both in generality and real scientific interest. Indeed, the visual environment depends not only on the DSF's characteristics but also on the configuration of the indoor space (geometry, optical properties) and the exact position of the user. Furthermore, it is understood that the characteristics of the DSF impacting on the visual environment are those related to the optical properties of the system, such as the visual transmittance of the glass panes and roller screen. While it is trivial to demonstrate that several other quantities potentially affecting the thermal behaviour have no role in the determination of the visual environment.

3.4. Index for the sensitivity analysis

The method adopted in this study follows the technique outlined in [45,46] and explores a limited input space around a baseline case following a method where all parameters are modified by the same order of magnitude, i.e. by the same perturbation. Local sensitivity indices are defined as follows: consider a model with n independent inputs $X_i = 1, \ldots, n$. For a given value of X , the local sensitivity indices are proportional to the partial derivatives of the output y with respect to the chosen ith input parameter x_i (first-order sensitivity index):

$$S_i(t) = X_i \frac{\partial y_k(t)}{\partial X_i} \quad (1)$$

The sensitivity index is calculated for each hour of the annual simulation. To get a single value of each parameter, the impact of each parameter is then determined by using the distance of the sensitivity index, $S_{i,d}$, following Spitz et al. [45], and is calculated using the mean ($S_{i,m}$) and the standard deviation ($S_{i,std}$) of S_i over the considered (annual) period according to the following equation:

$$S_{i,d} = \sqrt{{S_{i,m}}^2 + {S_{i,std}}^2} \quad (2)$$

3.5. Challenges in modelling and simulation for sensitivity analysis in different BES tools

While comparing the possibilities for sensitivity analysis with the two selected BES tools, it was revealed that EnergyPlus has limited flexibility in defining input parameters. The shading device is EnergyPlus by a hardcoded default placed in the middle of the cavity when the airflow window module is used. The frame properties (ratio, U_f values) cannot be defined for each one of the two skins, but as one parameter for the whole element. Moreover, the inlet area, the inlet height, and the ventilation gap around the shading are not used in the model (Table 1).

When it comes to the sensitivity analysis, most parameters can be directly defined in the software tools except for the changes in the U-values and spectral properties which are calculated inputs. The U-value cannot directly be adjusted by ±10% in either software when using an advanced window modelling approach, as this performance value is calculated from the given spectral properties and conductivity values of the glazing panes. In IDA ICE, a layer-by-layer calculation is used, while in EnergyPlus an equivalent glazing is used for the internal pane. The variations for the U-value were implemented by adjusting either the emissivity values of the glazed layers and/or the gas in the cavity without changing the thickness or other features so that the reference value reaches the targeted value and the optical properties of the glazed system were not modified.

For the solar transmission (τ), reflectance (ρ) and absorption (α) values of the shading or glazing, no single value can be modified without adjusting the two others since $\tau + \rho + \alpha = 1$ in all cases.

Table 1
Parameters considered in the sensitivity analysis.

Parameter		Parameter Values			Unit of measurement	Parameter availability		ID in Fig. 2
		Baseline X_i	+10% $X_i + \Delta X_i$	−10% $X_i - \Delta X_i$		IDA ICE	EnergyPlus	
Geometrical parameters								
Depth of the cavity measured from glass to glass	d_{cav}	0.22	0.242	0.198	(m)	+	+	(a)
Position of the shading measured from the internal surface of the external skin glazing system	d_{sh}	0.073	0.0803	0.0657	(m)	+	d_{cav}*0.5 by default	(b)
Ventilation gap around the shading, all directions (Distance of shading edge from the edge of the window element)	$d_{sh,gap}$	0.03	0.033	0.027	(m)	+	N/A	(c)
Frame fraction of external window element	$f\%_{ext}$	10%	0.11	0.09	(%)	+	$F_{\%\_combined}$: Single frame is defined for	(d)
Frame fraction of internal window element	$f\%_{int}$	10%	0.11	0.09	(%)	+	the whole element	(e)
Recess depth of window (distance of window external surface to building face)	d_{recess}	0.22	0.242	0.198	(m)	+	+	(f)
Area of the inlet	A_{inlet}	0.015	0.0165	0.0135	(m^2)	+	N/A	(g)
Position of inlet measured from the floor level	h_{inlet}	0.05	0.055	0.045	(m)	+	N/A	(h)
Thermal and optical parameters								
Centre of glass heat transfer coefficient of exterior glazing calculated at reference conditions (ISO 15099)	U_{g_ext}	1.357	1.4927	1.2213	(W/m^2K)	+	+	*(i)*
Total energy (shortwave) transmittance of external glazing system	τ_{e,g_ext}	0.324	0.3564	0.2916	(−)	+	+	*(j)*
Centre of glass heat transfer coefficient of interior glazing system calculated at reference conditions (ISO 15099)	U_{g_int}	1.507	1.6577	1.3563	(W/m^2K)	+	+	*(l)*
Total energy (shortwave) transmittance of interior glazing system	τ_{e,g_int}	0.492	0.5412	0.4428	(−)	+	+	*(m)*
Total energy (shortwave) transmittance of shading	$\tau_{e,sh}$	0.2	0.22	0.18	(−)	+	+	*(o)*
Total energy (shortwave) reflection of shading	ρ_{sh}	0.7	0.77	0.63	(−)	+	+	*(p)*
Total energy (shortwave) absorption of shading	α_{sh}	0.1	0.11	0.09	(−)	+	+	*(q)*
Heat transfer coefficient of the frame of the exterior skin including linear heat transfer coefficients of the glazing edge (Ψ_g)	U_{f_ext}	2	2.2	1.8	(W/m^2K)	+	$U_{f\_combined}$: Single frame is defined for the whole element. Equivalent value of 1 W/m2K is used.	*(k)*
Heat transfer coefficient of the frame of the interior skin including linear heat transfer coefficients of glazing edge (Ψ_g)	U_{f_int}	2	2.2	1.8	(W/m^2K)	+		*(n)*
Airflow parameters								
Volumetric airflow rate in the cavity	V_{cav}	5.556	6.1116	5.0004	(L/s/unit)	+	+	*(r)*

Table 2
Definition of variants of solar properties, example.

	τ	ρ	α
$\tau_{e,sh}$	0.2	0.7	0.1
$\tau_{e,sh}$ - 10%	0.18	0.718	0.102

Hence, all three values were modified for each variant with the following method: e.g. in case τ is the assessed parameter, the difference in τ is added to ρ and α with the same proportion as their original value (Table 2).

IDA ICE uses a variable timestep to solve the equations, in which the timestep is adapted to the frequency content of the solution to optimize simulation time [47]. Using the default setting with a maximum of a 1.5 h timestep is acceptable for annual energy simulations, as the small differences in the hourly values due to the different timesteps of the different models will not cause bias in the results. However, for the sensitivity analysis, where the input values of the models have only small differences, the small inaccuracies of the hourly values will affect the overall results. Hence, the maximum timestep is set to 6 min for both tools.

4. Results and discussion

The results are presented analysing one PI (see Section 3.3 and Appendix B) at a time (Section 4.1 for T_{glass}, Section 4.2 for e^{+}_{24h}, and Section 4.3 for e^{-}_{24h}), with comparisons for different climates and orientations. Section 4.4 focuses on the inter-software comparison.

4.1. Internal glass temperature

Both optical and thermal properties of the glazing and the shading (when present) were sensitive parameters, although the order of the parameters slightly differed for the two software tools and case assessed. In IDA ICE (Fig. 3), when the shading was not activated, the solar transmittance of the external skin was the most sensitive parameter, followed by the U-value of the internal and external glazing, and then by the solar properties of the internal skin. When the shading system was activated, the shading reflectance became the most sensitive parameter, resulting in the solar transmission the external pane becoming less significant. Additionally, the U-values of the external and the internal glazing were also ranked as sensitive parameters.

Comparison of the orientations shows that the ranking of the parameters was the same for South, East and West orientations, while on the North orientation, the optical properties of the glazing and the shading (when present) had a relatively lower effect than the thermal properties of the glazing. U_{g_ext} then ranked up among the most sensitive parameter, both with (2nd place) and without (1st place) the shading device activated. It is also worth mentioning that while $V_{cav,}$ the ventilation airflow rate in the cavity, was only moderately sensitive for the former three orientations and ranked at the 7th place when the shading is activated, the relative lower sensitivity of the optical properties of the glazing and shad-

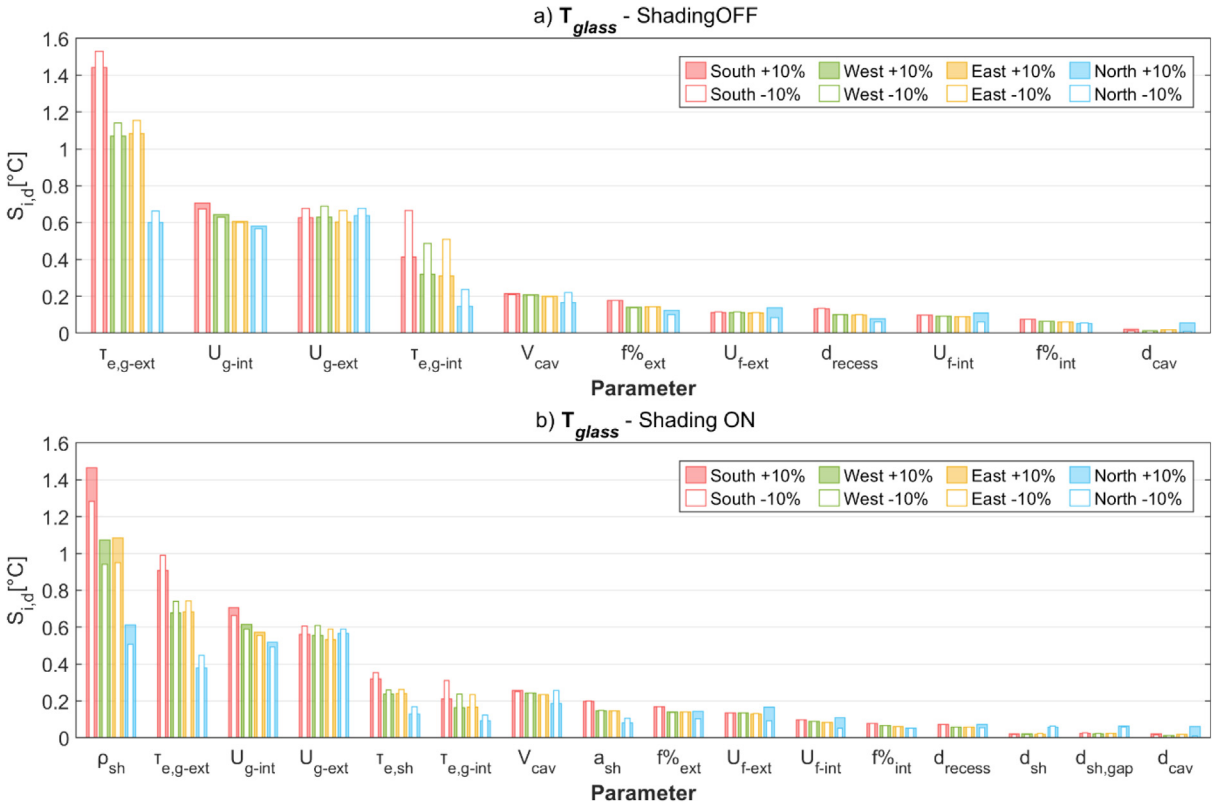

Fig. 3. $S_{i,d}$, Internal glazing temperature, Torino, all orientations, IDA ICE a) shading off b) shading on.

ing on the North orientation resulted in V_{cav} becoming the 5th most sensitive parameter, which was higher than the solar transmission of the shading and internal glazing.

In EnergyPlus (Fig. 4), the solar transmission of the internal glass was the most sensitive parameter when shading was not activated, followed by the solar transmission of the external glazing, and the U-values of both glazings and the cavity ventilation rate. With shading activated, the shading reflectance became the most sensitive parameter just like in IDA ICE, followed by the U-values of the internal glazing and the solar transmission of both glazings.

The comparison of the orientations shows that the ranking of the parameters was the same for most of the orientations. Like in IDA ICE, on the North orientation, the optical properties of the glazing and the shading had a relatively lower effect than the thermal properties of the glazing, thus resulting in U_{g_ext} as the second most sensitive parameter, both with and without the shading device activated.

The climate analysis showed that the most sensitive parameter was the same for all three locations for the South orientation with the only exception of U_{g_ext} becoming more sensitive in Oslo, and less sensitive in Hong Kong in the + 10% configuration (Fig. 5). On the North orientation, the most sensitive parameters showed a different behaviour in the various locations. The thermal properties of both glass panes and V_{cav} became significantly more sensitive in Oslo, and less sensitive for Hong Kong, both with and without the shading device activated. By contrast, the optical properties of the glazings and the shading device showed an opposite trend.

It is possible to conclude that in general terms, the indoor-side surface temperature of the DSF, which can play a role in terms of thermal comfort, is primarily affected by the optical properties of the glazed and shading layers, as well as by the thermal transmittance of the internal and external skin. Other parameters had a minimal impact on this variable, especially compared to the impact of the above-mentioned parameters.

4.2. Daily energy gain

e^{+}_{24h} was most sensitive to solar properties. As expected, when the shading was not activated in the cavity, the solar transmission of the external glazing was the most sensitive parameter, while when shading was activated, the shading solar reflection became the most sensitive parameter, as seen for T_{glass}. When the shading is off, in EnergyPlus, τ_{e,g_ext} was the only parameter with an outstandingly high $S_{i,d}$, and was more than three times higher than the $S_{i,d}$ of any other parameter which had a similarly low sensitivity (Fig. 7); IDA ICE (Fig. 6) also returned that the solar transmission of the external glazing was a parameter with high impact, closely followed by τ_{e,g_int}. With shading on, the difference between $\rho_{sh,}$ and the former parameters are lower for both tools.

For the daily energy gain, the comparison of the orientations showed that there were no notable differences in the ranking of the parameters.

The results of the climate analysis showed similarities results to those seen in the T_{glass} analysis (Fig. 8). The shading reflectance (when shading was activated) and the external glazing transmission were the most sensitive parameter for all three locations and all orientations, while the ranking of the parameters was only slightly affected by the change of the relative significance of U_{g_ext} on the South façade and both glazing U_g on the North façade.

In conclusion, the total daily heat gain, which affects the energy performance of the DSF in terms of cooling and heating loads, was driven by the optical properties of the external glazing such as the transmittance, and of the shading when present. Only one of the thermal properties, the thermal transmittance of the internal glazing, was significant but still had a somewhat limited impact. Over-

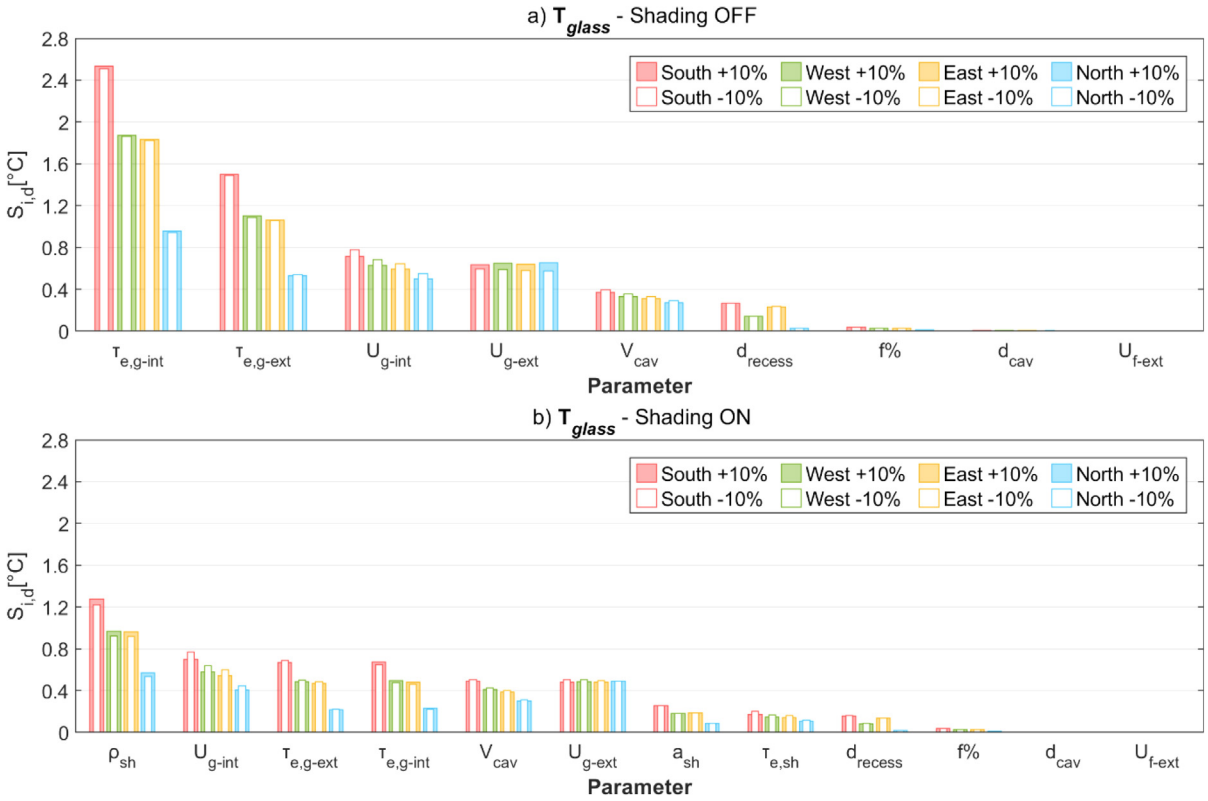

Fig. 4. S_{id}, Internal glazing temperature, Torino, all orientations, EnergyPlus a) shading off b) shading on.

all, the parameters with the highest impact were the same ones as those observed in the analysis of T_{glass} with the exception that when the shading was not activated, the role of the frame had more impact than the thermal properties of the glazing.

4.3. Daily energy loss

In the case of e^{-}_{24h} the most sensitive parameters were easily distinguished. In IDA ICE, the U-values of both glazings were significantly more sensitive than any other parameter, regardless of the presence of shading in the cavity or not (Fig. 9). In EnergyPlus, V_{cav} also appeared as one of the most sensitive parameters along with the U-values of the glazing (Fig. 10).

As previously seen for the energy gain, the most sensitive parameters for energy loss analysis were the same for all orientations.

Some minor changes can be seen in the ranking of this PI in different climates (Fig. 11), e.g. in Hong Kong, the frame fraction received a higher ranking than shading reflection; or in Oslo, τ_{e,g_ext} was ranked higher than in other climates for a North orientation when the shading device was deactivated. However, the list of the most sensitive parameters was not affected in any of the cases.

In conclusion, when it comes to the daily heat losses, which impact the DSF's energy performance through the heating load (i.e. primarily due to the behaviour during the night time and or in cold, cloudy winter days), the only relevant parameters were the thermal transmittance of the two skins and the airflow rate in the façade cavity.

4.4. Intersoftware comparison

As previously mentioned, the in-built model for the airflow window available in EnergyPlus requires a smaller amount of input than IDA ICE's but includes all of the parameters that were determined as the most sensitive in IDA ICE. These parameters are visible in Fig. 12 which also shows the results for a south-oriented façade in Turin.

For most parameters, the two tools have sensitivity indices in the same order of magnitude for T_{glass} and e^{+}_{24h}, with the only exception being the internal glass solar transmission. EnergyPlus shows a much higher sensitivity index for the T_{glass} while in IDA ICE, it is comparable in magnitude to the thermal properties of the glazing. In the case of e^{+}_{24h}, the behaviour of the tools was the opposite, with IDA ICE showing an almost four times bigger value then EnergyPlus.

For e^{-}_{24h} IDA ICE had higher $S_{i,d}$ values for most parameters, except for V_{cav}, where instead EnergyPlus returned higher variations compared to IDA ICE.

There is a significant difference in the weight of the solar transmission of the internal glazing, shading solar properties and airflow rate on the selected PIs. The solar transmission of the internal glazing had a significantly greater role in EnergyPlus than in IDA ICE for the glass temperature. This is anticipated to be due to the missing heat capacity node of the glass, as changing glazing solar properties will have an instantaneous effect on the glass pane temperature.

In EnergyPlus, V_{cav} is among the most sensitive parameters (3rd position) for e^{-}_{24h} and moderately sensitive for the other two PIs. However, in IDA ICE, it is only moderately sensitive for T_{glass} and e^{-}_{24h}, and even insensitive for e^{+}_{24h}. This indicates that the two tools calculate convective heat transfer coefficients differently, which also explains why there is a notable difference in the impact of the absorption of the shading.

It is particularly interesting that the cavity depth, d_{cav}, was found insensitive in both software tools and with all three PIs. Yet it is a reasonable outcome, as the analysed case is mechanically ventilated with fixed airflow rates, where the airflow rate is not dependent on this characteristic. The analysis reveals therefore

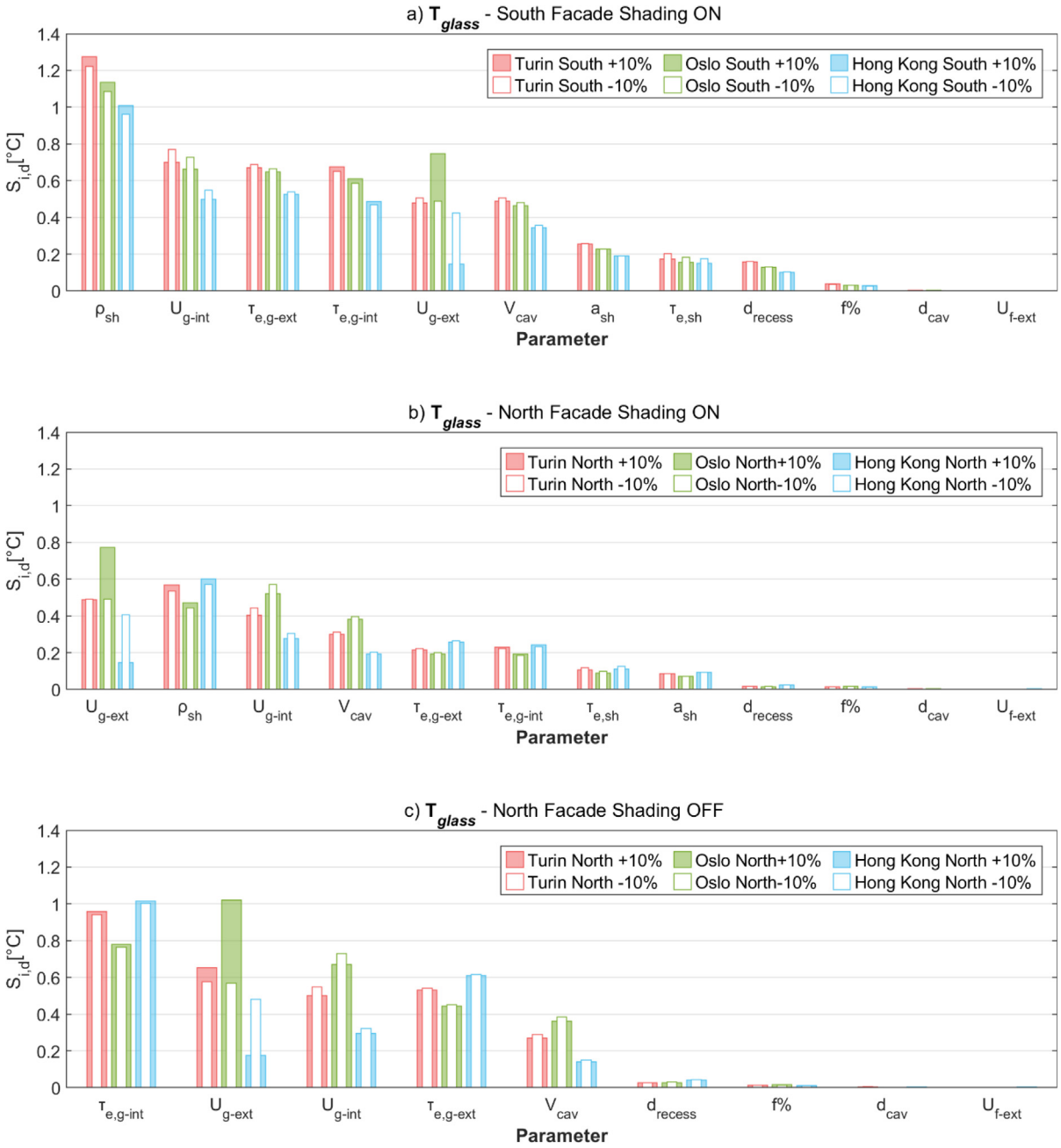

Fig. 5. S_{id}, Internal glazing temperature, all locations, EnergyPlus, a) South, shading on b) North, shading on, c) North, shading off.

that the cavity aspect ratio (cavity height over cavity depth) plays a marginal role when single-storey climate façade is assessed using the selected PI. The cavity depth affects the average velocity of the fluid given a fix airflow rate, and the average velocity of the fluid is a quantity used in the calculation of the convective heat exchange coefficient. This result shows that the models are not sensitive, at least in the explored range, to a small change in the convective heat exchange coefficient. In order to see a more relevant change in the fluid-dynamic characteristic of the cavity (at least as much as this domain is replicated by the models embedded in the BES tools), the airflow rate needs to change by at least of one order of magnitude. The insensitivity of the models is also seen when it comes to the inlet position and height (which is possible to implement in IDA ICE), which are instead parameters expected to be important in case of natural ventilation.

Regardless of the used software tools, some parameters had notable differences in the $S_{i,d}$ values resulting from the + 10% and −10% variations. This might indicate that the relationship between the parameter and the PI is non-linear in the evaluated input data region. These can be a subject for further analysis exploring the whole range of input space (e.g. the Morris method).

On a final note, even if not reported in this analysis, the height of the DSF can play a relevant role in the façade performance, both in terms of T_{glass} and in terms of e^{+}_{24h} and e^{-}_{24h}. However, this parameter is often not free to be decided by the designer or consultant, as it is often set due to other considerations than energy or environmental optimisation.

5. Conclusion

The comparison of the sensitivity of the results in IDA ICE and EnergyPlus showed that the ranking and magnitude of sensitivity indices were similar for most of the assessed parameters in the

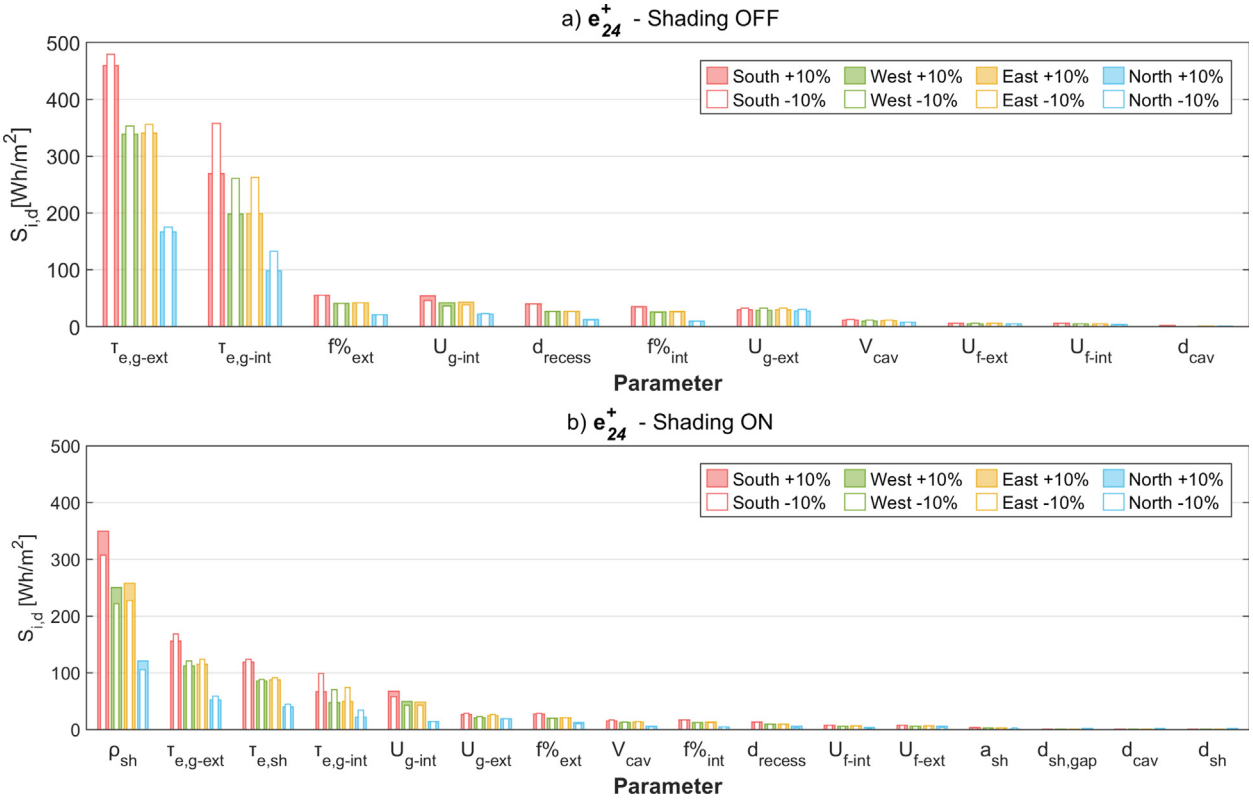

Fig. 6. S_{id}, Daily heat gain, Torino, all orientations, IDA ICE a) shading off b) shading on.

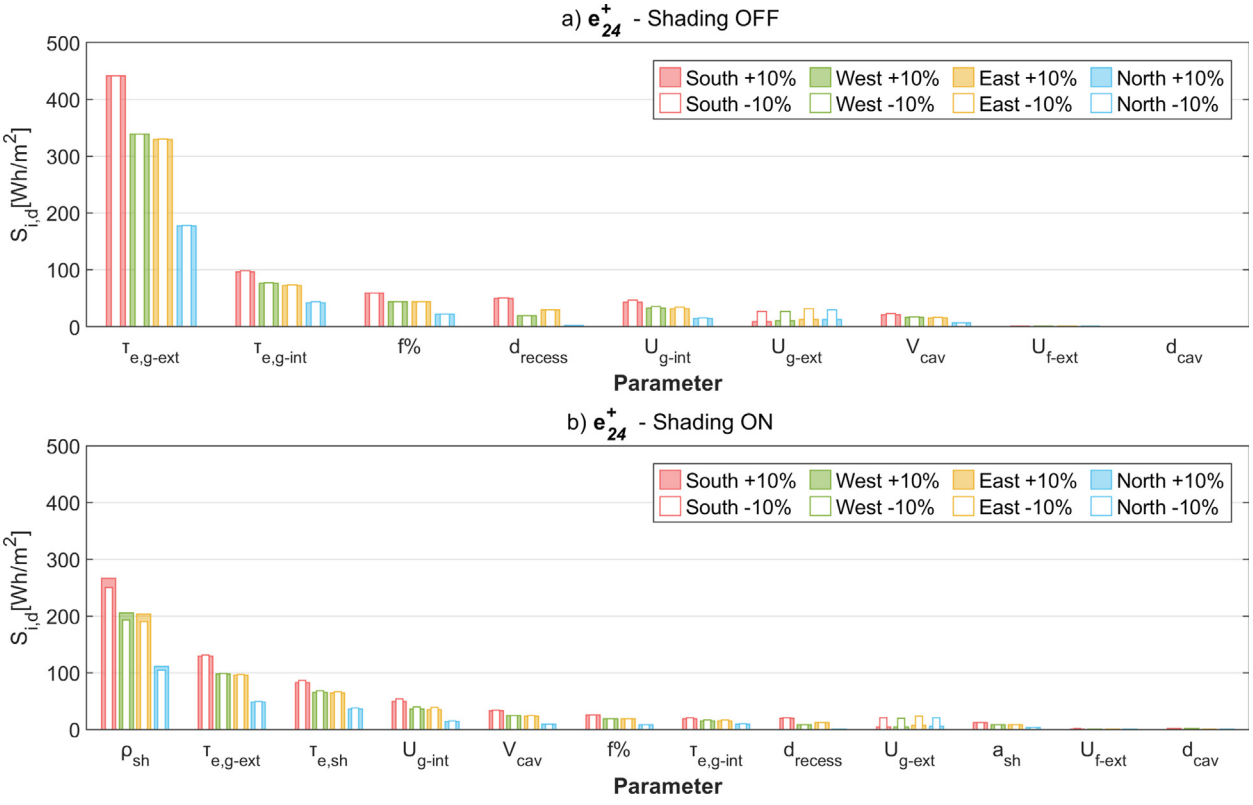

Fig. 7. S_{id}, Daily energy gain, Torino, all orientations, EnergyPlus a) shading off b) shading on.

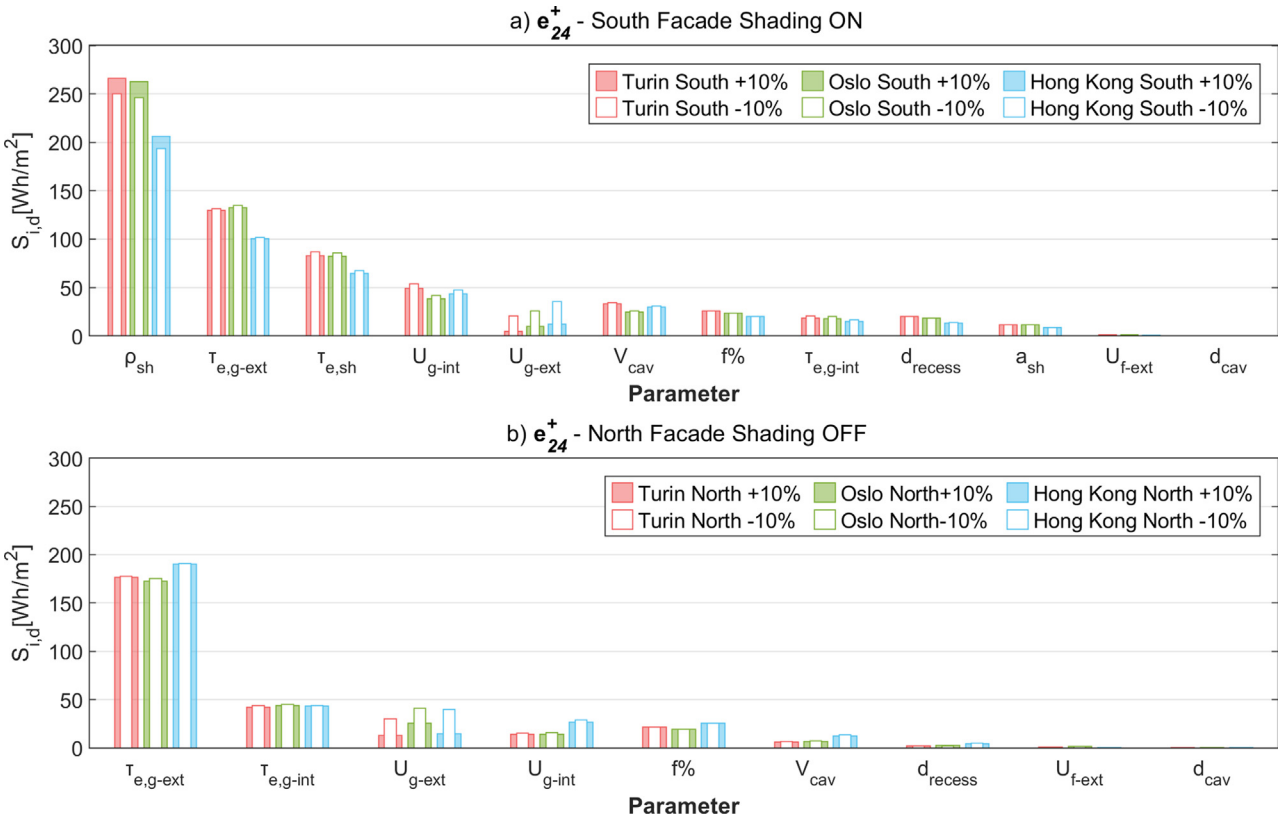

Fig. 8. S_{id}, Energy gain, all locations, EnergyPlus, a) South, shading on b) North, shading off.

Fig. 9. S_{id}, Daily heat loss, Torino, all orientations, IDA ICE a) shading off b) shading on.

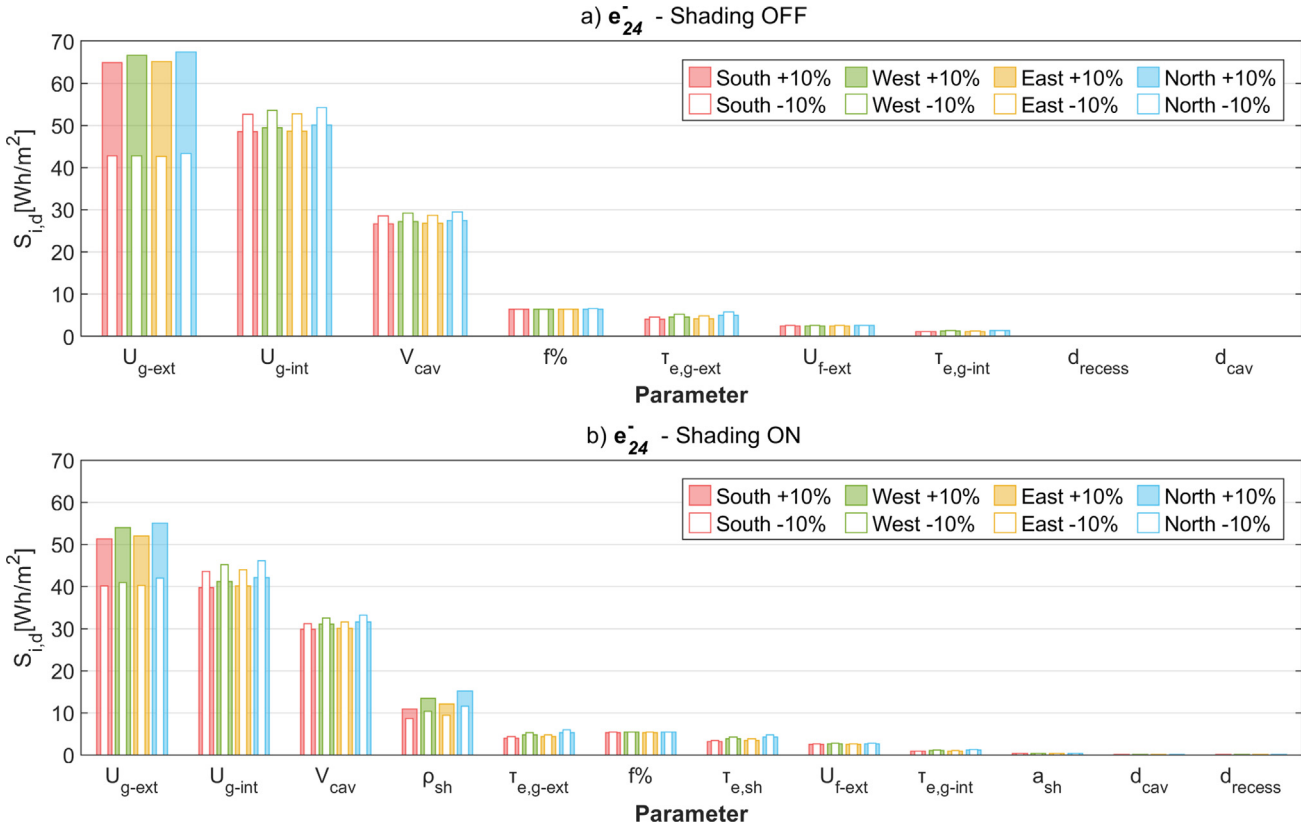

Fig. 10. S_{id}, Daily heat loss, Torino, all orientations, EnergyPlus a) shading off b) shading on.

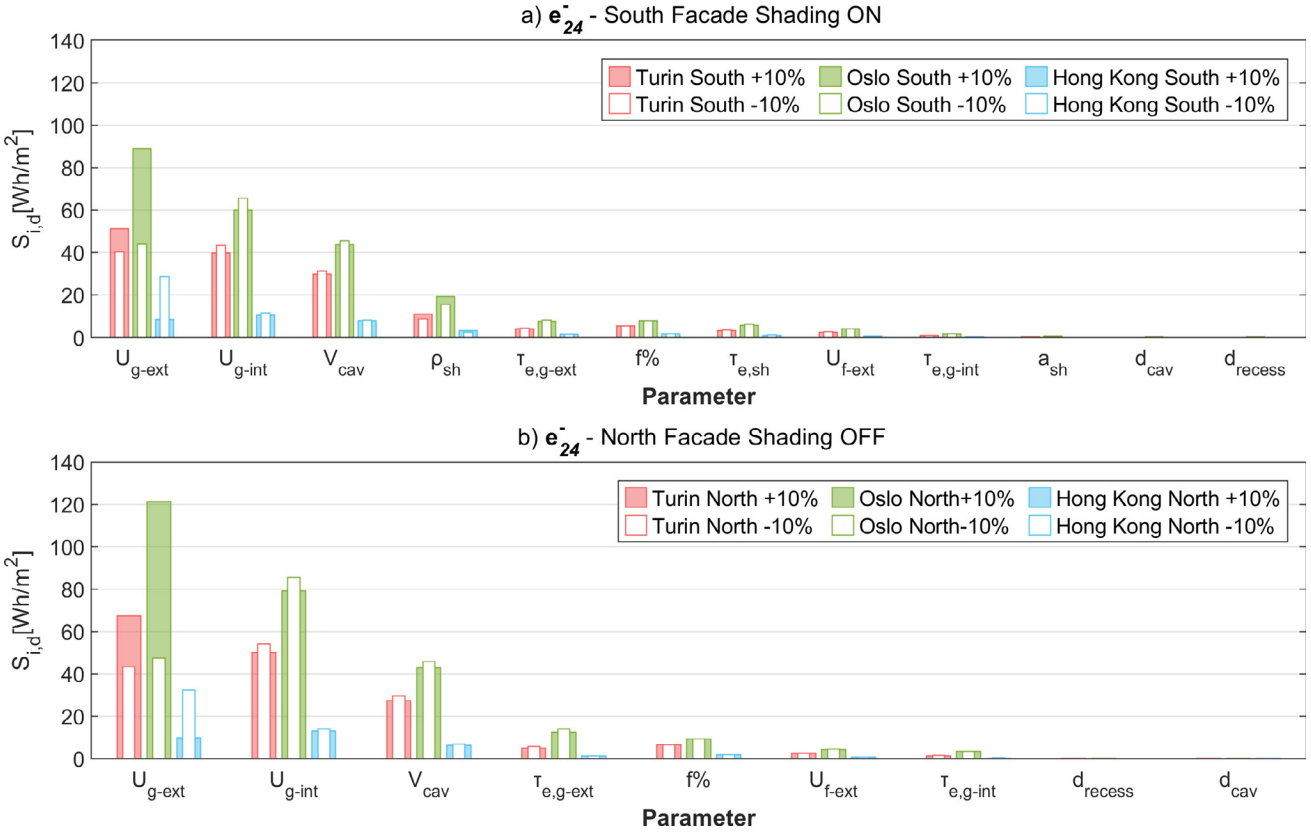

Fig. 11. Sid, Energy loss, all locations, EnergyPlus a) South, shading on b) North, shading off.

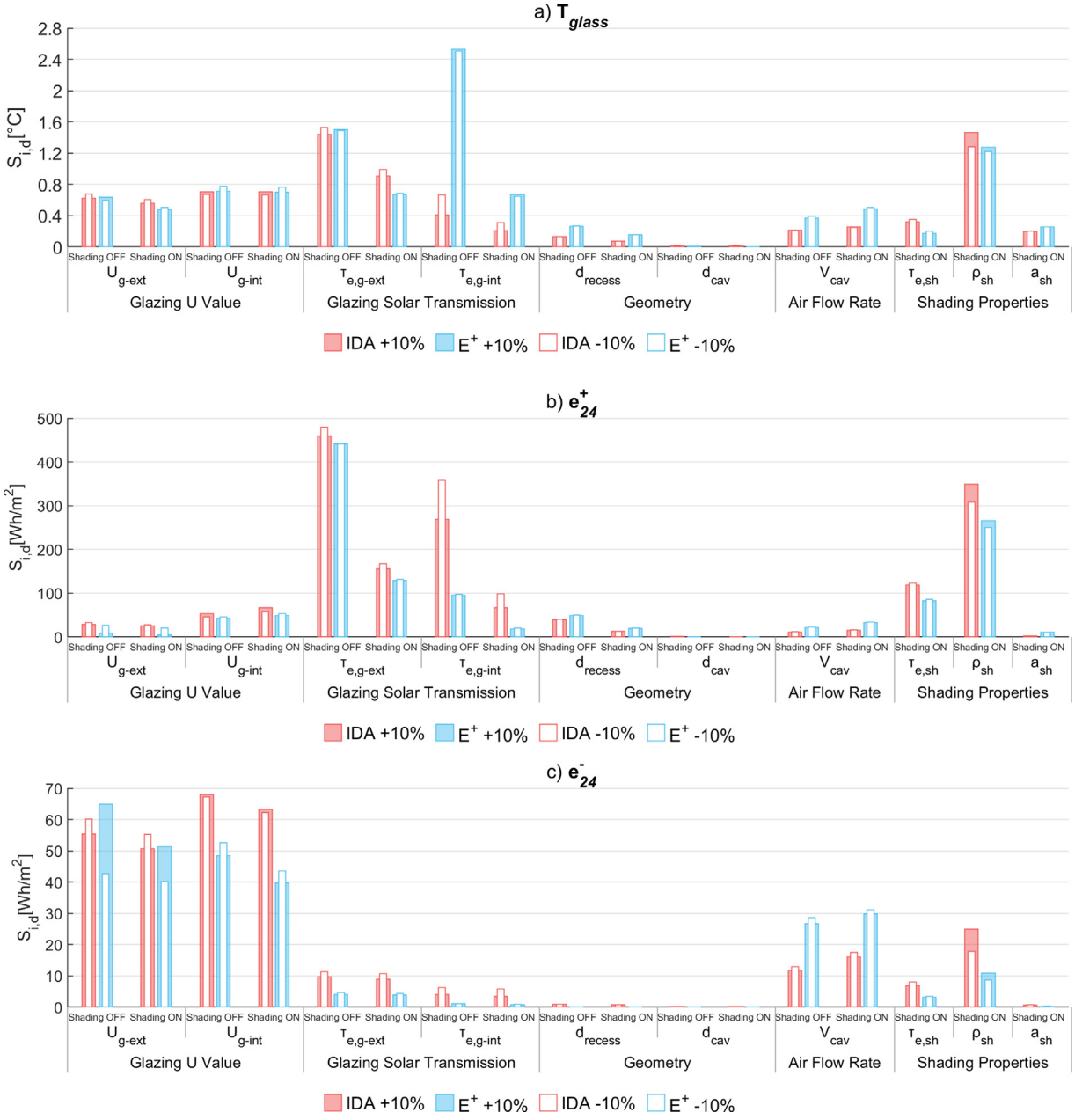

Fig. 12. Intersoftware comparison of $S_{i,ds}$ for IDA ICE and EnergyPlus: a) Internal glazing temperature b) Daily energy gain e^{+}_{24h} c) Daily energy loss e^{-}_{24h}.

two tools, with few exceptions. The general trend was that models were more sensitive to the parameters describing the glazing thermal and optical properties, and shading optical properties, when activated, than to the geometrical and frame properties. The effect of the airflow rate was, however, different in the two tools, as this parameter had a higher effect on the PIs in EnergyPlus. Additionally, the internal glazing temperature in EnergyPlus showed a higher sensitivity to the solar properties of the internal glazing than it did in IDA ICE. This can probably be explained by the missing heat capacity node in EnergyPlus. The models also showed moderate sensitivity to a variation in the air flow rate, which means that the convective heat exchange coefficients only had small variations within the investigated range. The airflow rate through a climate façade (that acts as an exhaust in the HVAC plant) is often determined by the necessary ventilation airflow rate due to the presence of occupants and a baseload. This value can to some extent be controlled (for example in combination with variable air volume systems) by reducing the air flow rate as a function of the actual environmental loads. However, for most of the applications, the allowed variation in the airflow to be explored in the design phase is usually small, as based on the design value assessed though standardised calculations, while the variation in the operation is normally not implemented. Within the possible small range of variation of the airflow rate, the performance of the climate façade is rather insensitive to this parameter. A different picture can be obtained when and if the climate façade is operated in a completely different way outside the occupancy time (e.g. during the night or the weekends) when the façade operates without forced airflow since the mechanical ventilation can be turned off – a strategy that is more likely to be adopted in highly efficient buildings.

The analysis showed that the ranking of the sensitivity indexes ($S_{i,d}$), is significantly different for each PI. However, the list of the most sensitive parameters for each PI remained the same for every

orientation and each climate, while minor differences occurred in the order of the moderately sensitive parameters.

In conclusion, the optical (solar transmittance) and thermal properties (thermal transmittance) of the glazing, and the optical properties (solar reflectance) of the shading systems adopted generated a larger variation on the selected performance parameters than those generated by other characteristics related to the geometrical features of the façade. This take-home lesson is important because it shows that the main constructional (size and airflow rate) characteristics of the climate façade can be fixed at the preliminary stage, when both the overall envelope vision and energy concept of the building is designed, without hindering the possibility to significantly modify the behaviour of the system at a later stage (by a careful selection of the glazed and shading layers). In a software tool perspective, the use of one or another tool should return the same results when it comes to selecting the optimal solution within a sensitivity analysis. While IDA ICE allows more inputs than EnergyPlus to be tested, the sensitivity analysis showed that this had little value since the most sensitive parameters are available in both tools.

CRediT authorship contribution statement

Adrienn Gelesz: Methodology, Formal analysis, Data curation, Software, Validation, Writing - original draft, Visualization, Funding acquisition. **Elena Catto Lucchino:** Methodology, Formal analysis, Data curation, Software, Validation, Writing - original draft, Visualization. **Francesco Goia:** Conceptualization, Methodology, Investigation, Validation, Writing - original draft, Funding acquisition, Project administration. **Valentina Serra:** Investigation, Writing - review & editing, Supervision. **András Reith:** Writing - review & editing, Supervision, Funding acquisition.

Declaration of Competing Interest

The authors declare that they have no known competing financial interests or personal relationships that could have appeared to influence the work reported in this paper.

Acknowledgements

The authors would like to thank the researchers and technical staff from Politecnico di Torino (Italy) involved in the experimental activity which provided the data used for model validation in this study.

Part of the activities presented in this paper were carried out within the research project "REsponsive, INtegrated, VENTilated - REINVENT – windows", led by the Norwegian University of Science and Technology (NTNU), supported by the Research Council of Norway through the research grant 262198, and research and industrial partners SINTEF, Hydro Extruded Solutions, Politecnico di Torino, and Aalto University.

The validation activity has been supported by the ÚNKP-18-3 New National Excellence Program of the Ministry of Human Capacities of Hungary.

The authors would like to thank Ellika Taveres-Cachat for proofreading the manuscript and improving its readability.

Appendix A

Airflow window – EnergyPlus model description

The built-in model adopted in Energy Plus is called 'Airflow Window'. This component allows the modelling of only mechanical ventilated façades. The model allows five different configurations for the airflow path, depending on which is the source and the destination of the forced air:

- Inside Air – Outside Air
- Inside Air – Inside Air
- Inside Air – Return Air
- Outside Air – Inside Air
- Outside Air – Outside Air

The configuration implemented in this study was the 'Inside Air-Outside Air' path because the return air was not used to climatize the indoor air.

This model adopts the calculation method described in the ISO Standard 15099 [48] for the ventilated gap. The following information is derived from the Engineering Reference of EnergyPlus [49].

Heat balance calculation

The window glass face temperatures are determined by solving the heat balance equations on each face of the glass at every time step.

The following assumptions are made in deriving the heat balance equations:

(1) The glass layers are thin enough (a few millimetres) that heat storage in the glass can be neglected; therefore, there are no heat capacity terms in the equations.
(2) The heat flow is perpendicular to the glass faces and is one dimensional.
(3) The glass layers are opaque to IR.
(4) The glass faces are isothermal. This is assumpted since the glass conductivity is usually very high.
(5) The short wave radiation absorbed in a glass layer can be distributed equally to the two faces of the layer.

The heat balance equations for the surfaces take into account the conductive, radiative and convection heat transfer of all the layers.

The heat balance equation for the external surface of 'Glass 1' in Fig. A1 is:

$$E_o\varepsilon_1 - \varepsilon_1\sigma\theta_1^4 + k_1(\theta_2 - \theta_1) + h_o(T_o - \theta_1) + S_1 = 0 \quad (A.1)$$

For the internal surface of 'Glass 1' is:

$$k_1(\theta_1 - \theta_2) + h_{cv}(T_{gap} - \theta_2) + \sigma\frac{\varepsilon_2\varepsilon_3}{1-(1-\varepsilon_2)(1-\varepsilon_3)}(\theta_3^4 - \theta_2^4) + S_2 = 0 \quad (A.2)$$

While for the internal surface of 'Glass 2':

$$k_2(\theta_4 - \theta_3) + h_{cv}(T_{gap} - \theta_3) + \sigma\frac{\varepsilon_2\varepsilon_3}{1-(1-\varepsilon_2)(1-\varepsilon_3)}(\theta_2^4 - \theta_3^4) + S_3 = 0 \quad (A.3)$$

And for the external surface of 'Glass 2':

$$E_i\varepsilon_4 - \varepsilon_4\sigma\theta_4^4 + k_2(\theta_3 - \theta_4) + h_i(T_i - \theta_4) + S_4 = 0 \quad (A.4)$$

where

ε = Emissivity of face i [–]
E_o, E_i = Exterior, interior long-wave radiation incident on window [W/m^2]
k_i = Conductance of glass layer i [W/ m^{2}K]
h_o, h_i = Outside, inside air film convective conductance [W/m^{2}K]

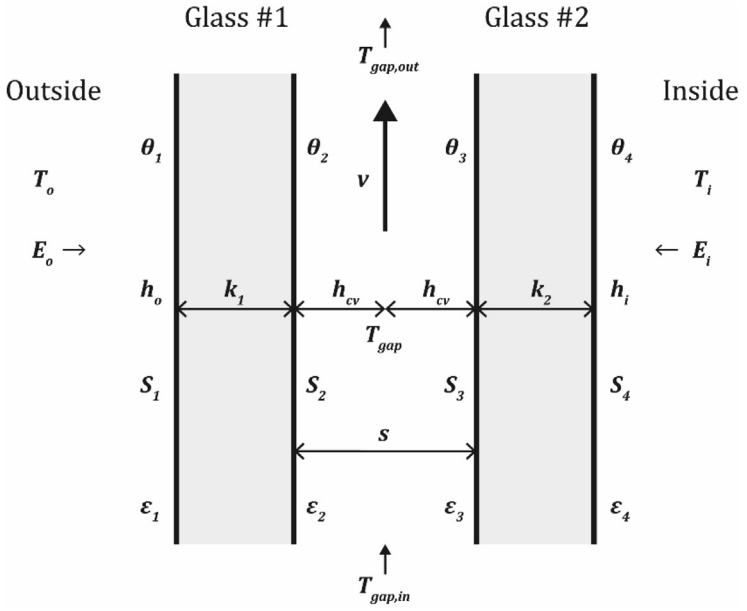

Fig. A1. Glazing system with forced airflow between two glass layers showing variables used in the heat balance equations [49].

h_{cv} = convective heat transfer coefficient from glass to gap air [W/m^{2}K]
θ_i = temperature of face i [K]
T_o, T_i = Outdoor and indoor air temperatures [K]
T_{gap} = effective mean temperature of the gap air [K]
σ = Stefan-Boltzmann constant [W/m^{2}K^4]
S_i = Radiation (short-wave, and longwave) absorbed by the ith glazing layer [W/m^2]

The convective heat transfer coefficient of both surfaces facing the same cavity is considered to be equal and given by:

$$h_{cv} = 2h_c + 4v \tag{A.5}$$

where

h_c = glass-to-glass heat transfer coefficient for non-vented (closed) cavity [W/m^{2}K] and calculated according to the ISO Standard 15099
v = air velocity in the gap (m/s) and it is calculated as

$$v = \frac{F}{A_{gap}} \tag{A.6}$$

where

F = airflow rate (m^3/s) which is assumed to be uniform across the width of the window.
A_{gap} = gap cross-sectional area in direction of flow (m^2)

The mean temperature of the gap air is given by the following expression:

$$T_{gap} = T_{ave} - \frac{H}{H_0}\left(T_{gap,out} - T_{gap,in}\right) \tag{A.7}$$

where

$$T_{ave} = \frac{\theta_2 + \theta_3}{2} \tag{A.8}$$

$$H_0 = \frac{\rho C_p s}{2h_{cv}} v \tag{A.9}$$

H = glazing height (m)
$T_{gap,in}$ = gap air inlet temperature (T_i if the airflow source is indoor air, T_o if the airflow source is outside air) (K).

The outlet air temperature is given by:

$$T_{gap,out} = T_{ave} - \left(T_{ave} - T_{gap,in}\right)e^{-H/H_0} \tag{A.10}$$

In the overall balance, the fan energy used to move air through the gap is ignored since is very.

In case of a shading device in the cavity (Fig. A2), the heat balance equations are the same as those for the between-glass shading device with natural convection. For each layer (glass or shading) the heat balance equations take also into account the energy reflected, absorbed and transmitted by the shading device.

For the internal surface of 'Glass 1' is:

$$\begin{aligned} &k_1(\theta_1 - \theta_2) + h_{cv,1}\left(T_{gap,1} - \theta_2\right) \\ &+ \frac{\sigma\varepsilon_2}{1-\rho_2 R_1}\left[\frac{\tau_{sh}}{1-\rho_6\rho_3}\left(\varepsilon_3\theta_3^4 + \varepsilon_6\theta_6^4\rho_3\right) + \varepsilon_5\theta_5^4 + \varepsilon_2\theta_2^4 R_1\right] \\ &- \sigma\varepsilon_2\theta_2^4 + S_2 \\ &= 0 \end{aligned} \tag{A.11}$$

For the shading layer surface facing 'Gap 1':

$$\begin{aligned} &k_{sh}(\theta_6 - \theta_5) + h_{cv,1}\left(T_{gap,1} - \theta_5\right) \\ &+ \frac{\sigma\varepsilon_5}{1-\rho_2 R_1}\left[\frac{\tau_{sh}\rho_2}{1-\rho_5\rho_3}\left(\varepsilon_3\theta_3^4 + \varepsilon_6\theta_6^4\rho_3\right) + \varepsilon_2\theta_2^4 + \varepsilon_5\theta_5^4\rho_2\right] \\ &- \sigma\varepsilon_5\theta_5^4 + S_5 \\ &= 0 \end{aligned} \tag{A.12}$$

with

$$R_1 = \rho_5 + \frac{\tau_{sh}^2\rho_3}{1-\rho_6\rho_3} \tag{A.13}$$

where

k_{sh} = Conductance of shading layer [W/ m^{2}K]

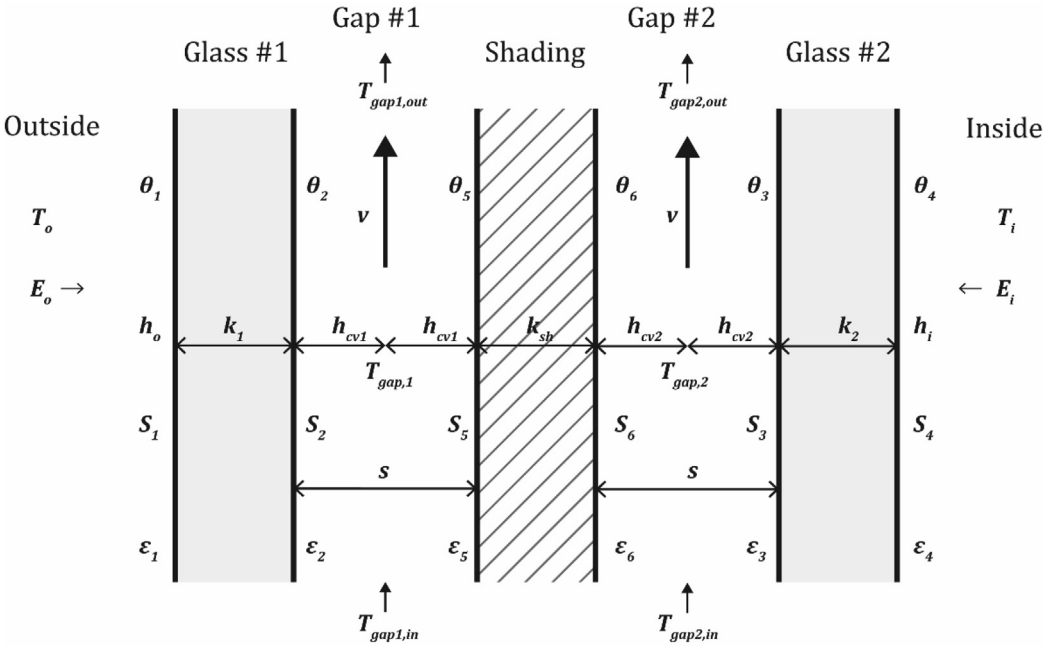

Fig. A2. Airflow window with between-glass shading device showing variables used in the heat balance equations [49].

τ_{sh} = IR diffuse transmittance of shading device
$\varepsilon_{sh(5,6)}$ = diffuse emissivity of shading device
$\rho_{sh(5,6)}$ = IR diffuse reflectance of shading device (=1 - (τ_{sh} + ε_{sh}))
$\theta_{sh(5,6)}$ = temperature of the surface of the shading layer that faces the gap (K).

The term 1 - $\rho_{sh}\rho_{glass}$ accounts for the inter-reflection of IR radiation between glass and shading layer.

To determine the gap air velocity, gap air mean-equivalent temperature and gap outlet air temperature a pressure-balance set of equations is used. The pressure balance equals the buoyancy pressure acting on the gap air to the pressure losses associated with gap airflow between gap inlet and outlet. The balance equations account for the two air gaps generated by the presence of the shading device in the cavity [48].

The heat convective coefficient of each gap is:

$$h_{cv,1} = 2h_{c,1} + 4v$$

$$h_{cv,2} = 2h_{c,2} + 4v \quad \text{(A.14)}$$

where

$h_{c,1}$, $h_{c,2}$ = surface-to-surface heat transfer coefficients for gap #1 and #2, respectively, when these gaps are non-vented (closed).
v = air velocity in the gap (m/s) and it is calculated as

$$v = \frac{F/2}{A_{gap}} \quad \text{(A.15)}$$

where

A_{gap} = sW is the cross-sectional area of the gap on either side of the shading device. It is assumed that the shading device is centred between the two panes of glass so that the airflow, F, is divided equally between the two gaps.

The average temperature of the two outlet air streams is:

$$T_{gap,ave,out} = (T_{gap,1,out} + T_{gap,2,out})/2 \quad \text{(A.16)}$$

Glazing system optical properties

In EnergyPlus, the optical properties of individual glass layers are given by the following quantities at normal incidence as a function of wavelength:

- Transmittance, T
- Front reflectance, R_f
- Back reflectance, R_b

The optical properties of a glazing system consisting of N glass layers separated by nonabsorbing gas layers are determined by solving the following recursion relations for $T_{i;j}$, the transmittance through layers i to j; $R^f_{i;j}$ and $R^b_{i;j}$, the front and back reflectance, respectively, from layers i to j; and A_j , the absorption in layer j.

For the case of double glazing (Fig. A3) this mean:

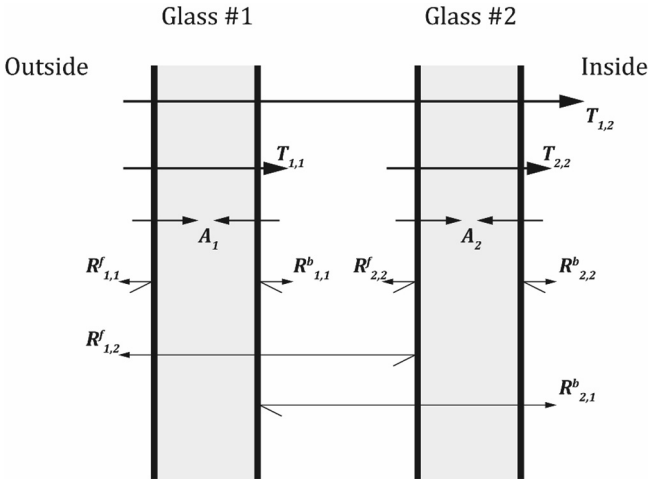

Fig. A3. Schematic of transmission, reflection and absorption of solar radiation within a multilayerglazing system [49].

$$T_{1,2} = \frac{T_{1,1}T_{2,2}}{1 - R^f_{2,2}R^b_{1,1}} \tag{A.17}$$

$$R^f_{1,2} = R^f_{1,1} + \frac{T^2_{1,1}R^f_{2,2}}{1 - R^f_{2,2}R^b_{1,1}} \tag{A.18}$$

$$R^b_{2,1} = R^b_{2,2} + \frac{T^2_{2,2}R^f_{1,1}}{1 - R^b_{1,1}R^f_{2,2}} \tag{A.19}$$

$$A_1 = (1 - T_{1,1} - R^f_{1,1}) + \frac{T_{1,1}R^f_{2,2}(1 - T_{1,1} - R^b_{1,1})}{1 - R^f_{2,2}R^b_{1,1}} \tag{A.20}$$

$$A_2 = \frac{T_{1,1}(1 - T_{2,2} - R^b_{2,2})}{1 - R^f_{2,2}R^b_{1,1}} \tag{A.21}$$

These relations account for multiple internal reflections within the glazing system. If the above transmittance and reflectance properties are input as a function of wavelength, EnergyPlus calculates "spectral average" values of the above glazing system properties by integrating over wavelength.es is a function of wavelength. The angular properties are calculated as a function of the angle of incidence. Two different methods apply if the glass is coated or uncoated.

Shading device optical properties

Shading devices affect the system transmittance and glass layer absorptance for short-wave radiation and long-wave (thermal) radiation. The effect depends on the shade position (interior, exterior or between-glass), its transmittance, and the amount of interreflection between the shading device and the glazing. Also of interest, it is the amount of radiation absorbed by the shading device. The shading device implemented in the model used for this study is the type "shades". "Shades" are assumed to be perfect diffusers. This means that direct radiation incident on the shade is reflected and transmitted as hemispherically uniform diffuse radiation: there is no direct component of transmitted radiation. It is also assumed that the transmittance, τ_{sh}, reflectance, ρ_{sh}, and absorptance, α_{sh}, are the same for the front and back of the shade and are independent of angle of incidence.

The optical properties, both shortwave and longwave, of the glazing system (with the shading device) are calculated as a function of the isolated shade properties (i.e., shade properties in the absence of the glazing) and the isolated glazing properties (i.e., glazing properties in the absence of the shade).

Double glass façade (DgFacade) – IDA ICE model description

The double skin façade was modelled as a Detailed Window model and a custom component called Double Glass Facade (DgFacade) attached to it (Fig. A4). These modules can model the connection of the air inlet and outlet both towards the indoor environment and to the outside. A forced flow rate can be assigned to it if the façade is connected to the HVAC system.

The façade cavity is partitioned vertically and horizontally, surrounded in all directions by air spaces with identical conditions. Both horizontal and vertical partitions are transparent to the incoming solar radiation, and heat flux through them is neglected [50]. The shading device, if present, can be assigned to both glazings. In the presented work, the shading has been assigned to the external glazing, as interior shade. The inner façade can also include opaque parts as well, which are considered in the heat balance equations.

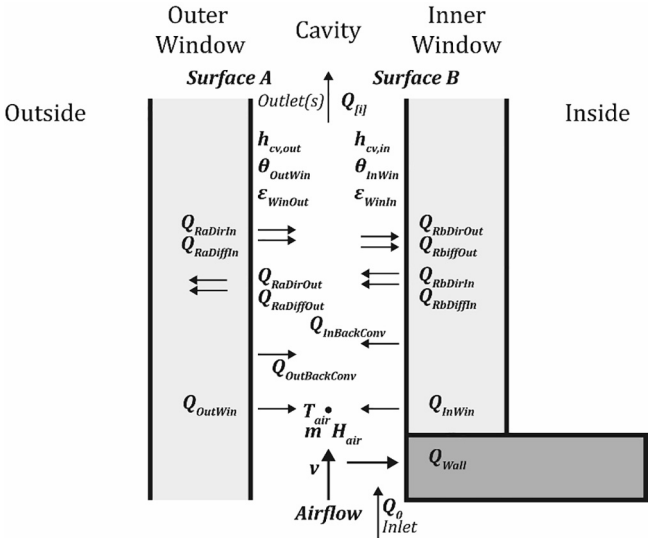

Fig. A4. Model of the DbFacade.

The Detailed Window Model follows the ISO 15099 [48] calculation method described above.

Energy balance at the window surfaces

The heat flux to the windows from the double façade is the sum of the convective heat flux and the longwave heat flux at the window surfaces.

For inner window:

$$Q_{InWin} = Q_{conv,InWin} + Q_{LW,InWin} \tag{A.22}$$

For outer window:

$$Q_{OutWin} = Q_{conv,OutWin} - \Sigma Q_{LW,wall} - Q_{LW,InWin} \tag{A.23}$$

where

Q_{InWin} = heat flux into the inner window from double façade [W]
$Q_{conv,InWin}$ = convective heat flux from the inner window [W]
$Q_{LW,InWin}$ = Longwave heat flux from the inner window [W]
Q_{OutWin} = heat flux to the outer window from the double façade [W]
$Q_{conv,OutWin}$ = convective heat flux from the outer window [W]
$\Sigma Q_{LW,Wall}$ = Longwave heat flux from the wall (currently 0) [W]

Energy balance of the cavity air

The air enthalpy gain is calculated as a combination of the convective heat gain from the windows and the wall, the back convection from the shaded window(s) and the heat flow from the terminals. Moisture balance and CO_2 balance is calculated in each timestep as well, and the mass of the air is calculated with "RhoMois" – function from the air temperature and humidity.

$$m\frac{\partial H_{air}}{\partial t} = Q_{ConvOutWin} + Q_{ConvInWin} + Q_{ConvWallTot} + Q_{OutBackCv} + Q_{InBackCv} + Q_0 + \sum_{i=1}^{nTerminals} Q[i] \tag{A.24}$$

$$m = \rho V \tag{A.25}$$

where

m = mass of air [kg]

ρ = density [kg/m^3]
V = volume of cavity air [m^3]
H_{air} = air enthalpy [J/kg]
$Q_{OutBackCv}$ = heat flow from outside curtain back convection [W]
$Q_{InBackCv}$ = heat flow from inside curtain back convection [W]
$Q_{ConvWallTot}$ = convective heat flux from wall [W]
Q_0 = heat flux from term_0 [W]
Q_i = heat flux from term_i [W]

The vertical temperature gradient of the air space is neglected as the air is considered well mixed.

Convection

Convective heat gain is calculated as follows:

$$Q_{conv,InWin} = h_{cv,InWin} A_{InWin} (\theta_{InWin} - T_{air}) \quad (A.26)$$

Where

θ_{InWin} = temperature of the inner window surface [K]
T_{air} = air temperature in the gap [K]
h_{cv} = surface convective heat transfer coefficient [W/m^{2}K]
A_{InWin} = surface of the inner window [m^2]

Convection from surfaces is treated as non-linearly using standard ICE natural convection function called *u_film*. The convective heat transfer coefficients in the DBfacade model follow equation (A.27). The value is chosen for each window surface (external glazing and the cavity, when no shading is present/between the shading and cavity when present, and the internal glazing and the cavity) from the greater of the convective heat transfer coefficient from natural and forced airflow:

$$h_{cv} = \max\left(h_{cv,forced}; h_{cv,nat}\right) \quad (A.27)$$

where

$h_{cv,forced}$ = surface convective heat transfer coefficient calculated for forced convection [W/m^{2}K]
$h_{cv,nat}$ = surface convective heat transfer coefficient for natural convection [W/m^{2}K]

The forced convection heat transfer function is taken from the VDI Heat Atlas [51]. First, the Reynold's number is calculated, that is used then to calculate the Nusselt number. Both laminar flow and turbulent flow can be considered, depending on the cavity geometry and airspeed. The calculation method for the natural convection follows the Detailed Natural Convection Algorithm (DNCA), depending on the temperature difference of the surface and the air, and also the inclination of the surface (surface slope = 0 for floor and 180 for ceiling) (Table A1).
where

v = airspeed [m/s]
l = *height of the cavity [m]*
$\cdot$ = dynamic viscosity of the air [N s/m^2]
Re = Reynolds number
λ = thermal conductivity of the air [W/m^2]
Pr = Prandtl-number

The convection in the enclosed gaps of the glazing and between the shading and the external glazing is defined in the Detailed Window Model, that follows ISO 15099 [48]. The convection heat gain between the back surface of the shading and the shaded window(s) is considered in the ventilated cavity air heat balance.

Table A1
Equations used for calculating convective heat transfer coefficients within the ventilated window model.

Natural flow (DNCA)		Forced flow	
If $\Delta T < 0$ K and surface	slope < 90 °Or $\Delta T > 0$ K and surface slope > 90°		
	$h_{nat,conv} = \frac{9.482 \cdot \lvert\Delta T\rvert^{1/3}}{7.823 - \lvert\cos\left(\pi \cdot \frac{\beta}{180}\right)\rvert}$	$h_{conv,forced} = Nu * \frac{\lambda}{l}$ $Re = lv\frac{\rho}{\eta}$	
Else	$h_{nat,conv} = \frac{1.81 \cdot \lvert\Delta T\rvert^{1/3}}{1.382 + \lvert\cos\left(\pi \cdot \frac{\beta}{180}\right)\rvert}$	if, Re < 10^4 (laminar flow)	$Nu = 0.664 \cdot \sqrt{Re} \cdot Pr^{\frac{1}{3}}$
		if Re > 10^4: (turbulent flow)	$Nu = \frac{0.037 \cdot Re^{0.8} \cdot Pr}{1 + 2.443 \cdot Re^{-0.1} \cdot (Pr^{\frac{2}{3}} - 1)}$

Long-wave radiation

Long-wave radiation is treated with the full non-linear Stefan-Boltzmann relations and view factors between the surfaces.

$$Q_{LW,InWin} = \frac{1}{\frac{1}{\varepsilon_{Winln}} + \frac{1}{\varepsilon_{WinOut}} - 1} A\sigma \cdot \lvert((\theta_{InWin} - 273K)^2 + (\theta_{OutWin} - 273K)^2) \cdot ((\theta_{InWin} - 273K) + (\theta_{OutWin} - 273K)) \cdot (\theta_{InWin} - \theta_{OutWin})\rvert \quad (A.28)$$

where

ε = Emissivity of face i [–]
θ_i = temperature of face i [K]
σ = Stefan-Boltzmann constant [W/m^{2}K^4]

Solar radiation

Entering direct and diffuse short-wave radiation is absorbed first by the outer window, then by the eventual shading and then by the inner window (Calculations based on ISO 15099 [48]). The inner window is shaded first by any surrounding buildings (standard ICE function), then by the shading device.

At the beginning of the calculation, the actual shading factors are precomputed for all (plausible) solar locations and stored as parameters in the shading model connected to each window/opening [47]. The fraction of radiation (k) reaching each window and surface is calculated, both for diffuse and direct radiation, with the help of the *Shading, Winlight, Lightfract models.* The first reflection is captured by the model.

Once the radiation hits a window, the whole surface of the window is considered as the diffuse or direct radiation source, not just the lit portion of this surface, that is not shaded by external objects. The exact target location of the transmitted direct light beam is computed, the reflected portion spread diffusely. Reflected short wave radiation is assumed to be diffusely distributed according to surface view factors, the window is radiating with equal intensity, not considering the position of the direct radiation falling on the surface. [47]

Radiation heat balance of cavity surfaces:

$$Q_{ra,dir,out} = Q_{rb,dir,in} \quad (A.29)$$

$$Q_{ra,diff,out} = Q_{rb,diff,in} + Q_{SW,ref,tot} \quad (A.30)$$

Calculation of the radiation from the external window:

$$Q_{rb,dir,out} = k_{dir} \cdot Q_{ra,dir,in} \quad (A.31)$$

$$Q_{rb,diff,out} = k_{diff} \cdot Q_{ra,diff,in} \quad (A.32)$$

where

k_{diff} = Fraction of diffuse radiation to the inner window
k_{dir} = Fraction of direct radiation to the inner window
$Q_{ra,dir,out}$ = leaving direct solar radiation through surface A (outer window)
$Q_{rb,dir,in}$ = entering solar radiation from surface B (inner window)
$Q_{ra,diff,out}$ = leaving diffuse solar radiation through surface A (outer window)
$Q_{rb,diff,in}$ = entering diffuse solar radiation from surface B (outer window)
$Q_{SW,ref,tot}$ = radion reflected backwards from the outer window

Airflow

The airflow through the air space is driven by the density difference between space and ambient air. Intake and exhaust air grilles are assumed to be at the floor and ceiling level respectively. A leakage path between the room and the air space is also provided (in a separate model). All airflows can have arbitrary directions, bidirectional transport of energy, humidity and mass fraction is possible through the openings. Pressure drop in the intake and exhaust grilles is modelled in separate leak models (which may be controlled by specific signals)

$$\dot{m}_0 + \sum_{i=1}^{nTerminals} m[i] = 0 \tag{A.33}$$

where

$\dot{m}_0$ = mass flow from terminal 0

Since the shading device is assigned to the external window, the airflow between the external glass and the shading is calculated within the Detailed Window Model.

Appendix B

Experimental analysis for software tools validation

A full-scale office room with two exhaust-air façade modules located in a temperate sub-continental climate location in northern Italy (45° N latitude) was continuously monitored for around two years, as more extensively described in [3,52]. The test cell consisted of one zone representing an office space (H × W × D = 3.4 m × 3.2 m × 6.5 m) and two DSF modules (1.60 m wide, 3.40 m high) on the (almost exactly) south-exposed façade. Each DSF had a mechanically ventilated cavity, where the indoor air flowed into the cavity from a bottom opening and was extracted through a duct, placed at the top of the ventilated gap. The Climate façade configuration under investigation in this paper had a double glazed unit in both the internal and external skin, and a controllable, highly reflective roller blind placed at approximately one-third of the cavity, measured from the exterior glazing unit (Fig. B1).

During the long-term measurements, the indoor temperature was maintained at the desired setpoint of 20 °C in winter and 26 °C in summer by means of a combined air system and ceiling radiant panel. The test cell and the modules were equipped with a wide range of sensors: thermocouples for surface and air temperature measurements, heat flux meter sensors, pyranometers both inside and outside. Sensors were placed in several heights (+1,00, +2,00, +3,00 m) both inside and outside of the façade. The procedures adopted for data acquisition, sensors positions and considerations on the influence of sensors on the acquired values are not here detailed for the sake of brevity but follows the same methods and analyses presented in [53]. The measurement accuracies of the sensors and the measurement chain were: ±0.3 °C, ±5% and ±5%, for thermocouples, heat flux meters (hourly values) and pyranometers (hourly values), respectively (Table B1).

This accuracy led to the estimation of the uncertainty on the daily energy flows through the façade to be around 30% due to error propagation in data postprocessing (data aggregation to obtain daily energy flows through the façade, as described more in details in Section 3.3. More details on the experimental analysis can be found in [52] and are not herewith given for the sake of brevity.

Software tools validation procedures and key performance indicators

The validation through comparison with experimental data was carried out over four different weeks. The selected periods included two weeks (one in summer and one in winter) with shading up (OFF) and two weeks (one in summer and one in winter) with shading down (ON). These weeks had temperature peaks (low/high) and solar irradiation peaks representative for the corresponding season. Moreover, each period included both sunny and warm days, and sunny and cold days, as well as overcast sky conditions.

The validation of the two BES tools was performed at the façade level, and not at room level. Interest was placed on the reliability of the DSF model and not on the entire BES tool. Thus, the measured and simulated quantities that are compared are related to the DSF alone and not to the system "façade-plus-room". Since the BES tools were already validated in all the other parts against several standards –e.g. EN 15255-2007, Envelope BESTEST, etc–, only the performances of the sub-models representing the DSF were assessed.

The validation was carried out by comparing the measured data with the results of the simulations. Using the recorded experimental data, a weather data file (based on the original EnergyPlus Weather Data for the location of the experiment) was created to replicate the boundary conditions occurred during the experiments. Outdoor air temperature, global and beam solar irradiation were changed in the weather data file to allow the simulations to be done with input data derived from the measurement.

The validation procedure was based on the comparison of two types of PIs, which were later used in the sensitivity analysis. The PIs were selected to be representative of the thermal and comfort performance of the façade. The daily energy across the façade, specified as daily heat gain e^{+}_{24h} [Wh/m^2] and daily heat loss e^{-}_{24h} [Wh/m^2] were used to assess the sensitivity of the parameters when considering the energy performance of the DSF. The surface temperature of the indoor-facing surface of the inner skin, T_{glass} [°C], was instead used to assess the sensitivity of the parameters that affect the indoor thermal comfort.

While the surface temperature is a rather straightforward quantity, the daily heat gain and loss were obtained as described in Eqs. (B.1)–(B.3), where $I_{tr}(t)$ was the transmitted solar radiation, and $\dot{q}_{LW,conv}(t)$ was the sum of the longwave radiation and convective heat flux at the surface of the innermost glass pane, facing the indoors.

Hourly heat transfer:

$$\dot{q}_{tot}(t) = I_{tr}(t) + \dot{q}_{LW,conv}(t) \tag{B.1}$$

Daily heat gain:

$$e^{+}_{24h} = \int_{00:00}^{00:00+1day} \dot{q}^{+}_{tot}(t)dt \tag{B.2}$$

Daily heat loss:

$$e^{-}_{24h} = \int_{00:00}^{00:00+1day} \dot{q}^{-}_{tot}(t)dt \tag{B.3}$$

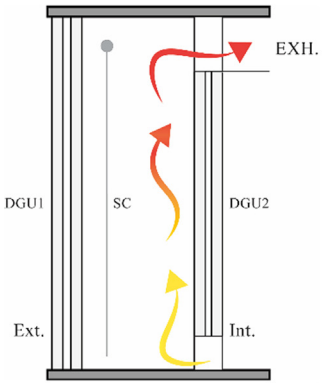

ID	Layers from exterior to interior	
DGU1	20 mm	Laminated, low-iron glass with selective coating, pos.2, 10.10.4
	16 mm	Air
	10 mm	Low-iron clear glass
SC		High reflectance roller blind
DGU2	10 mm	Low-e clear glass pos.2
	16 mm	Air
	10 mm	Laminated clear glass 5.5.4

Fig. B1. Schematic section and glazing configuration of the DSFs.

Table B1
Experimental periods.

		WINTER		SUMMER	
	Week	1	2	3	4
Outdoor temperature [°C]	max	7	7	34	26
	min	−1	−1	17	12
	average	3	2	25	18
Shading device	ON	OFF	ON	OFF	
Max vertical outdoor irradiance [W/m^2]	866	880	641	797	
Daily horizontal irradiation [kWh/m^2]	max	2.34	1.75	6.92	5.33
	average	1.67	1.3	5.5	3.79
Daily vertical irradiation [kWh/m^2]	max	4.98	4.47	6.7	5.44
	average	2.72	2.6	3.75	3.58

Table B2
RMSE values for interior glazing surface temperature [°C]

	Winter		Summer	
	Shading down	Shading up	Shading down	Shading up
IDA ICE [°C]	0.7 °C	1.1 °C	0.6 °C	0.9 °C
EnergyPlus	2.0 °C	3.0 °C	1.6 °C	2.0 °C

From the measured experimental data, the PIs were calculated as described here below:

- The surface temperature of the indoor glass was calculated by area-weighted averaging the values measured at three heights.
- The daily energies were calculated using:
- The surface heat flux (combining the convective heat exchange and the long-wave radiative heat exchange) measured at the indoor surface of the interior glazing pane, calculated by area-weighted averaging the values measured at three heights.
- The vertical transmitted solar irradiance, measured at the middle of the DSF's height.

As for the outputs of the simulations, T_{glass} values were directly logged in both simulation tools, while the daily heat loss and gain were calculated as the following:

- In IDA ICE daily energy gain/loss were calculated from hourly values of the transmitted solar radiation through the glazing and heat flux (radiative long-wave and convective) exchanged at the internal surface of the glazing, as described above (Eqs. (B.1)– (B.3)):
- In EnergyPlus the following output variables were logged for daily energy values:
  - Daily heat gain is directly obtained from Surface Window Heat Gain Energy [J]
  - Daily heat loss is directly obtained from Surface Window Heat Loss Energy [J]

The validation was carried out qualitatively by comparing time evolution of the quantities, and also quantitatively, by means of the Root Mean Square Error (RMSE) as an indicator of fitness of the models with the experiments, as described in Eq. (B.4),

$$RMSE = \sqrt{\frac{1}{n}\sum_{i=1}^{n}(X_{sim} - X_{exp})^2} \quad \text{(B.4)}$$

where n is the number of measurements,X is the hourly value, the subscript *sim* is for the simulated value, *exp* is for the experimental value.

Results of the software tools validation

Indoor surface temperature

The time evolution of the quantities simulated by IDA ICE matched well the experimental values, while simulations in EnergyPlus returned a time shift in the peaks up to 3 h, compared to the experiments. IDA ICE underestimated peaks in summer and overestimated them in winter with an error in the range −2 °C to + 3

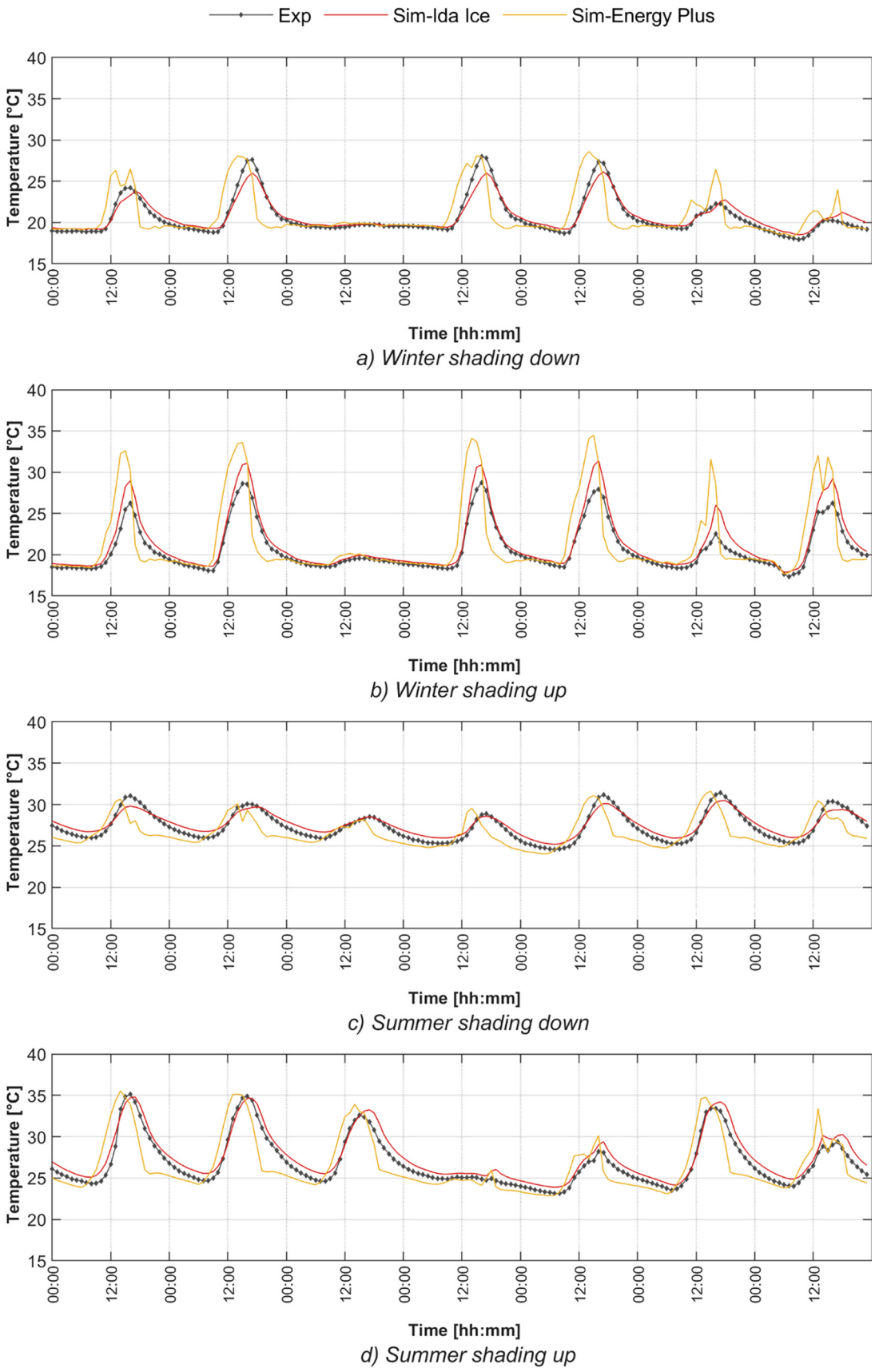

Fig. B2. Interior glazing surface temperature.

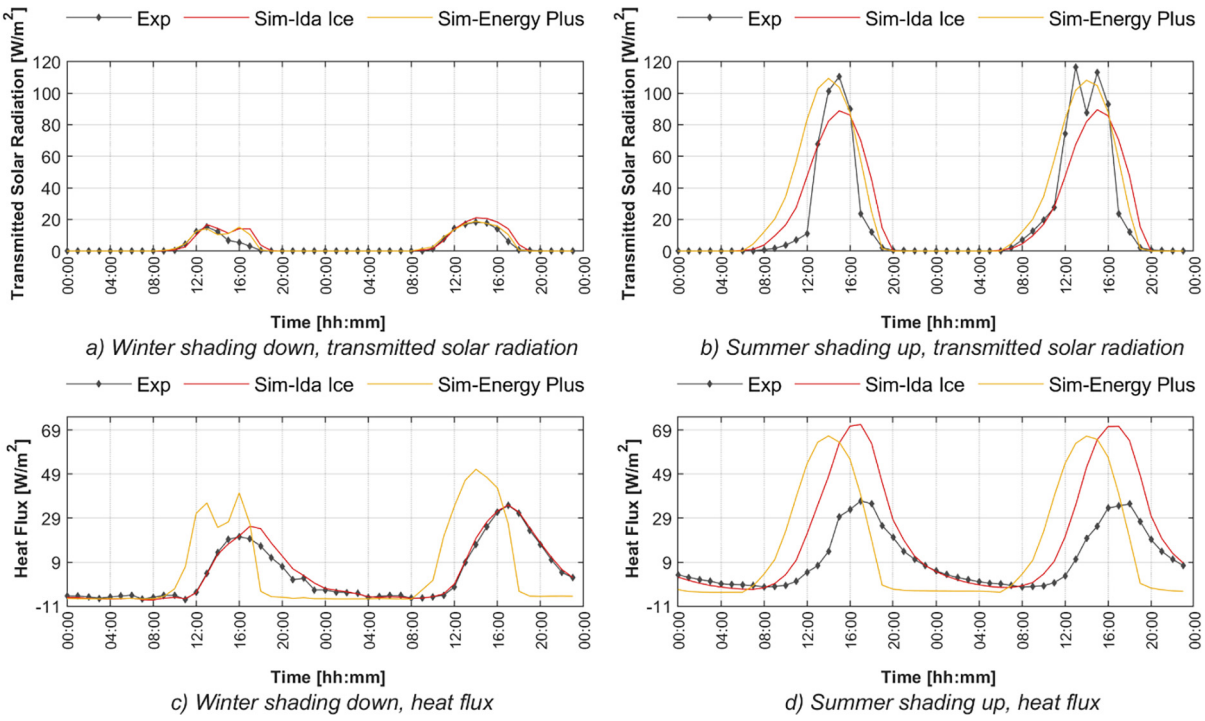

Fig. B3. Time profiles of transmitted solar radiation and heat flux for the first two days of two selected periods.

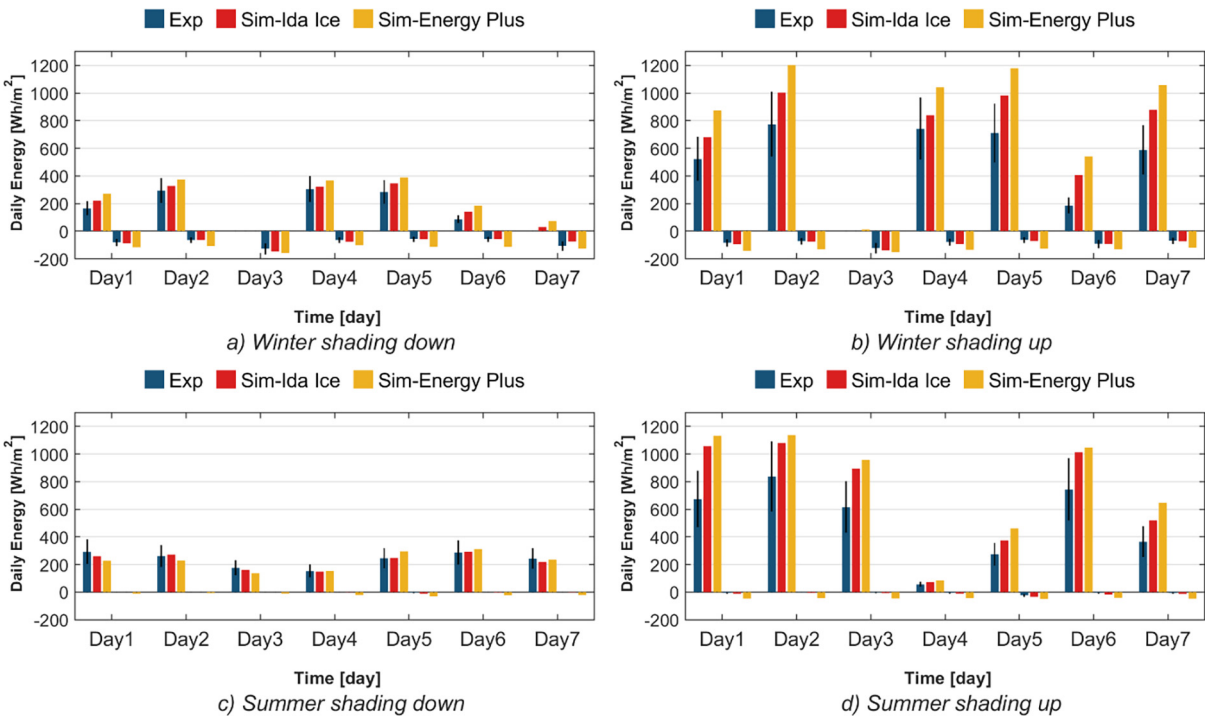

Fig. B4. Daily transmitted energy.

.5 °C. Minimum values were close to the experiments, with small overestimation, showing a maximum difference of nearly 0.9 °C. RMSE values were lower for IDA ICE in all periods compared to EnergyPlus. The latter often overestimated the values of the peaks, exceeding 10 °C when shading was disabled. Conversely, as for IDA ICE, the minimum values were close to the experiments, with a maximum difference of approximately 1 °C. In general, the errors in EnergyPlus were circa 1.5 °C greater than in IDA ICE (Table B2).

The main reason for the higher errors in EnergyPlus is due to the model of the glass panes. While IDA ICE includes a heat capacity

Table B3
RMSE values for Daily transmitted energy.

	Winter				Summer			
	Shading down		Shading up		Shading down		Shading up	
	IDA ICE	EnergyPlus	IDA ICE	EnergyPlus	IDA ICE	EnergyPlus	IDA ICE	EnergyPlus
e^{+}_{24h} [Wh/m^2]	43	83	205	371	17	37	237	299
e^{-}_{24h} [Wh/m^2]	15	42	11	53	3	18	8	38

node for the glazing, the thermal inertia of the glazing is not implemented in the EnergyPlus model. Hence, any heat absorbed by the glass surface shows an instantaneous effect on the glass temperature, causing a higher temperature rise than in reality. While one can be surprised to imagine such a large effect of the heat capacity of the glass panes, it is important to remember that the simulated system has a rather thick glass structure (50 mm of glass when both the exterior and the interior skin are considered). A conventional, single skin, glazing system is usually composed of a total thickness of glass in the range around 1 cm. Therefore, its inertial characteristics are relatively low, and the impact of this feature on the dynamics of the heat transfer rather limited – if not negligible. Conversely, in a double skin façade (with safety glass panes), the accounting of the heat absorbed and released because of the specific heat capacity of the material is no longer imperceptible. To highlight this effect, a simulation comparison was carried out by repeating a simulation in IDA ICE using the real value of the specific heat capacity of the glass and by setting a zero value. This investigation showed that when the specific heat capacity is neglected in IDA ICE, the simulation results in IDA ICE were extremely close to those obtained by EnergyPlus. On the contrary, when the specific heat capacity of the glass was used (and hence the system simulates correctly the effect of the heat capacity of the glazed system), the time evolution simulated by IDA ICE was much closer to the experimental data (as already shown Fig. B2 and B3c-3d), and different from the one calculated by EnergyPlus.

Daily transmitted energy

The transmitted energy was calculated from the transmitted solar radiation component and the long-wave and convective heat flux at the internal glass surface. The time profiles of these two components are shown to understand the causes of the deviations if present (Fig. B3).

While the time profiles and values of the solar radiation followed the experimental values generally well, with some differences in case of the shading being absent, the heat flux showed higher differences for the same periods (Fig. B4).

Despite the differences in the values and time profiles of solar transmission and heat flux, the general trend of the area-specific energy gain e^{+}_{24h} and heat loss e^{-}_{24h} was captured in a rather similarly by both software tools. However, the accuracy of the simulation tools seems to be strongly related to the simulated configuration: when the shading was in use (and hence all the heat gain and loss reduced), both tools returned results that are within the experimental uncertainty range; conversely, when the DSF was simulated without the roller screen, the inaccuracy increased considerably. In wintertime, the two tools had rather similar performances. Their results were mostly within the experimental error range. In the summer, there was a clearer difference between the two tools, with IDA ICE performing better then EnergyPlus which constantly overestimated the heat gain, surpassing the maximum values of the experimental errors. In general, e^{-}_{24h} had much lower RMSE values (Table B3), but this is also due to the much less intense values for this variable when compared to e^{+}_{24h}. In periods with shading up, e^{+}_{24h} was often highly overestimated in both tools, and up to almost twice the measured values when the simulation was carried out with EnergyPlus in the summer season. This latter discrepancy can be inferred to be primarily due to the lack of the capacitive node in EnergyPlus's model. While such a simplification is usually of little relevance in traditional windows characterised by few and thin glass layers, the effects of multiple and rather thick glass layers usually seen in DSF systems are not properly replicated by the available model.

Errors were higher for heat gains, and especially during days with high solar radiation. Apart from the model simplifications (as described in the article main body), the high deviation of heat flux values was, to some extent, caused by procedures and practices adopted in the measurements. When solar radiation is present, the measurement devices for temperature and heat flux could heat up, affecting the measured values. For this reason, dedicated shielding solutions [54] were implemented in the experimental campaign [52]. However, these solutions determine a local change of the thermophysical behaviour near the measurement points. While for temperature sensors such an approach usually leads to rather accurate results, when applied to heat flux sensors, it can result in an excessive influence on the thermophysical phenomena under assessment.

References

[1] F. Pomponi, P.A.E. Piroozfar, R. Southall, P. Ashton, E.R.P. Farr, Energy performance of Double-Skin Façades in temperate climates: A systematic review and meta-analysis, Renew. Sustain. Energy Rev. 54 (2016) 1525–1536, https://doi.org/10.1016/j.rser.2015.10.075.

[2] E. Catto Lucchino, F. Goia, G. Lobaccaro, G. Chaudhary, Modelling of double skin facades in whole-building energy simulation tools: A review of current practices and possibilities for future developments, Build. Simul. 12 (2019) 3–27, https://doi.org/10.1007/s12273-019-0511-y.

[3] A. Gelesz, E. Catto Lucchino, F. Goia, A. Reith, V. Serra, Reliability And Sensitivity Of Building Performance Simulation Tools In Simulating Mechanically Ventilated Double Skin Facades, in: V. Corrado, A. Gasparella (Eds.), Proc. Build. Simul. 2019 16th Conf. IBPSA, Rome, 2019.

[4] A. De Gracia, A. Castell, L. Navarro, E. Oró, L.F. Cabeza, Numerical modelling of ventilated facades: a review, Renew. Sustain. Energy Rev. 22 (2013) 539–549, https://doi.org/10.1016/j.rser.2013.02.029.

[5] C. Underwood, F. Yik, Modelling Methods for Energy in Buildings, John Wiley & Sons, 2008.

[6] B. Bueno, M. Street, T. Pflug, C. Braesch, A co-simulation modelling approach for the assessment of a ventilated double-skin complex fenestration system coupled with a compact fan-coil unit, Energy Build. 151 (2017) 18–27, https://doi.org/10.1016/j.enbuild.2017.04.029.

[7] A. De Gracia, L. Navarro, A. Castell, L.F. Cabeza, Numerical study on the thermal performance of a ventilated facade with PCM, Appl. Therm. Eng. 61 (2013) 372–380, https://doi.org/10.1016/j.applthermaleng.2013.07.035.

[8] A. Hazem, M. Ameghchouche, C. Bougriou, A numerical analysis of the air ventilation management and assessment of the behavior of double skin facades, Energy Build. 102 (2015) 225–236, https://doi.org/10.1016/j.enbuild.2015.05.057.

[9] N. Safer, M. Woloszyn, J.J. Roux, Three-dimensional simulation with a CFD tool of the airflow phenomena in single floor double-skin facade equipped with a venetian blind, Sol. Energy. 79 (2005) 193–203, https://doi.org/10.1016/j.solener.2004.09.016.

[10] D. Angeli, A. Dama, Modelling natural ventilation in double skin facade, Energy Procedia. 78 (2015) 1537–1542, https://doi.org/10.1016/j.egypro.2015.11.186.

[11] A. Dama, D. Angeli, O. Kalyanova Larsen, Naturally ventilated double-skin façade in modeling and experiments, Energy Build. 114 (2017) 17–29.

[12] A. Gelesz, Á. Bognár, A. Reith, Effect of shading control on the energy savings of an adaptable ventilation mode double skin facade, in: 13th Conf. Adv. Build. Ski. 1-2 Oct. 2018, Bern, Switz. - Prog., 2018.

[13] A. Alberto, N.M.M. Ramos, R.M.S.F. Almeida, Parametric study of double-skin facades performance in mild climate countries, J. Build. Eng. 12 (2017) 87–98, https://doi.org/10.1016/j.jobe.2017.05.013.
[14] T. Saroglou, T. Theodosiou, B. Givoni, I.A. Meir, Studies on the optimum double-skin curtain wall design for high-rise buildings in the Mediterranean climate, Energy Build. 208 (2020), https://doi.org/10.1016/j.enbuild.2019.109641 109641.
[15] R. Høseggen, B.J. Wachenfeldt, S.O. Hanssen, R. Hoseggen, B.J. Wachenfeldt, S. O. Hanssen, Building simulation as an assisting tool in decision making. Case study: With or without a double-skin facade?, Energy Build 40 (2008) 821–827, https://doi.org/10.1016/j.enbuild.2007.05.015.
[16] N. Hamza, Double versus single skin facades in hot arid areas, Energy Build. 40 (2008) 240–248, https://doi.org/10.1016/j.enbuild.2007.02.025.
[17] A.L.S. Chan, T.T. Chow, K.F. Fong, Z. Lin, Investigation on energy performance of double skin façade in Hong Kong, Energy Build. 41 (2009) 1135–1142, https://doi.org/10.1016/j.enbuild.2009.05.012.
[18] M. Ghadimi, H. Ghadamian, A.A. Hamidi, M. Shakouri, S. Ghahremanian, Numerical analysis and parametric study of the thermal behavior in multiple-skin façades, Energy Build. 67 (2013) 44–55.
[19] M.H. Tascon, Experimental and computational evaluation of thermal performance and overheating in double skin façades, (2008) 370.
[20] A. Malkawi, Y.K. Yi, A Method for Evaluating the Efficiency of Double-skin Facades, (n.d.) 1–8.
[21] H. Poirazis, Double skin façade glazed office buildings ; A parametric study for optimized energy and thermal comfort performance, 2 (2007) 797–801.
[22] M.H.H. Tascon, Experimental and Computational Evaluation of Thermal Performance and Overheating in Double Skin Facades, University of Nottingham, 2008.
[23] J. Joe, W. Choi, Y. Kwak, J.H. Huh, Optimal design of a multi-story double skin facade, Energy Build. 76 (2014) 143–150, https://doi.org/10.1016/j.enbuild.2014.03.002.
[24] D. Saelens, Energy performance assessment of single storey multiple-skin facades, 2002. https://doi.org/Ph. D. thesis.
[25] M.H. Tascon, CFD SIMULATION OF A DOUBLE SKIN FAÇADE MODEL, (2006).
[26] I. Pérez-Grande, J. Meseguer, G. Alonso, Influence of glass properties on the performance of double-glazed facades, Appl. Therm. Eng. 25 (2005) 3163–3175, https://doi.org/10.1016/j.applthermaleng.2005.04.004.
[27] E. Gratia, A. De Herde, The most efficient position of shading devices in a double-skin facade, Energy Build. 39 (2007) 364–373, https://doi.org/10.1016/j.enbuild.2006.09.001.
[28] H. Poirazis, Double skin façade cavities; a parametric study, in: Glas. Perform. Days 2007, 2007: pp. 271–275.
[29] A. Gelesz, A. Reith, Classification and re-evaluation of double-skin facades, Int. Rev. Appl. Sci. Eng. 2 (2011) 129–136, https://doi.org/10.1556/IRASE.2.2011.2.9.
[30] W.J. Stec, Symbiosis of double skin facade and indoor climate installation, Technische Universiteit Delft (2006).
[31] A.S. Anđelković, I. Mujan, S. Dakić, Experimental validation of a EnergyPlus model: Application of a multi-storey naturally ventilated double skin façade, Energy Build. 118 (2016) 27–36, https://doi.org/10.1016/j.enbuild.2016.02.045.
[32] N.M. Mateus, A. Pinto, G.C. Da Graça, Validation of EnergyPlus thermal simulation of a double skin naturally and mechanically ventilated test cell, Energy Build. 75 (2014) 511–522, https://doi.org/10.1016/j.enbuild.2014.02.043.
[33] D.W. Kim, C.S. Park, Difficulties and limitations in performance simulation of a double skin façade with EnergyPlus, Energy Build. 43 (2011) 3635–3645, https://doi.org/10.1016/j.enbuild.2011.09.038.
[34] A. Gelesz, Sensitivity of exhaust-air façade performance prediction to modelling approaches in IDA ICE, Int. Rev. Appl. Sci. Eng. 10 (2019) 241–252.
[35] A. Gelesz, A. Reith, Climate-based performance evaluation of double skin facades by building energy modelling in Central Europe, in, Energy Procedia (2015) 555–560, https://doi.org/10.1016/j.egypro.2015.11.735.
[36] O. Kalyanova, P. Heiselberg, Empirical Validation of Building Simulation Software, Modeling of Double Facades (2008).
[37] M.H. Kristensen, S. Petersen, Choosing the appropriate sensitivity analysis method for building energy model-based investigations, Energy Build. 130 (2016) 166–176, https://doi.org/10.1016/j.enbuild.2016.08.038.
[38] J.C. Lam, S.C.M. Hui, Sensitivity analysis of energy performance of office buildings, Build. Environ. 31 (1996) 27–39, https://doi.org/10.1016/0360-1323(95)00031-3.
[39] K. Petr, J. Filip, K. Karel, H. Jan, Technique of uncertainty and sensitivity analysis for sustainable building energy systems performance calculations, IBPSA 2007 - Int, Build. Perform. Simul. Assoc. 2007 (2007) 629–636.
[40] W. Tian, A review of sensitivity analysis methods in building energy analysis, Renew. Sustain. Energy Rev. 20 (2013) 411–419, https://doi.org/10.1016/j.rser.2012.12.014.
[41] C.J. Hopfe, J.L.M. Hensen, Uncertainty analysis in building performance simulation for design support, Energy Build. 43 (2011) 2798–2805, https://doi.org/10.1016/j.enbuild.2011.06.034.
[42] D.M. Hamby, A Review of Techniques for Parameter Sensitivity Analysis of Environmental Models, Environ. Monit. Assess. 32 (1994) 135–154.
[43] S. Petersen, M.H. Kristensen, M.D. Knudsen, Prerequisites for reliable sensitivity analysis of a high fidelity building energy model, Energy Build. 183 (2019) 1–16, https://doi.org/10.1016/j.enbuild.2018.10.035.
[44] K. Menberg, Y. Heo, R. Choudhary, Sensitivity analysis methods for building energy models: Comparing computational costs and extractable information, Energy Build. 133 (2016) 433–445, https://doi.org/10.1016/j.enbuild.2016.10.005.
[45] C. Spitz, L. Mora, E. Wurtz, A. Jay, Practical application of uncertainty analysis and sensitivity analysis on an experimental house, Energy Build. 55 (2012) 459–470, https://doi.org/10.1016/j.enbuild.2012.08.013.
[46] G. Cattarin, L. Pagliano, F. Causone, A. Kindinis, F. Goia, S. Carlucci, C. Schlemminger, Empirical validation and local sensitivity analysis of a lumped-parameter thermal model of an outdoor test cell, Build. Environ. (2018), https://doi.org/10.1016/j.buildenv.2017.12.029.
[47] Equa AB, EQUA Simulation AB User Manual IDA Indoor Climate and Energy, (2013).
[48] International Organisation for Standardisation, ISO 15099:2003 Thermal performance of windows, doors and shading devices - detailed calculations, 2003.
[49] U.S. Department of Energy, Engineering Reference 8.8, (2017).
[50] Equa AB, IDA – Indoor Climate and Energy ver 3.0 NMF-model documentation, (n.d.).
[51] VDI Heat Atlas, 2010. https://doi.org/10.1007/978-3-540-77877-6.
[52] F. Goia, L. Bianco, M. Perino, V. Serra, Energy performance assessment of and advanced integrated facade through experimental data analysis, Energy Procedia. 48 (2014) 1262–1271, https://doi.org/10.1016/j.egypro.2014.02.143.
[53] F. Goia, V. Serra, Analysis of a non-calorimetric method for assessment of in-situ thermal transmittance and solar factor of glazed systems, Sol. Energy. (2018), https://doi.org/10.1016/j.solener.2018.03.058.
[54] O. Kalyanova, F. Zanghirella, P. Heiselberg, M. Perino, R. Jensen, Measuring air temperature in glazed ventilated façades in the presence of direct solar irradiation, in: Proc. Roomvent 2007 - 10th 7th Int. Conf. Air Distrib. Rooms, Helsinki, 2007: pp. 209–218.